Earth Systems and Environment (2025) 9:541–562
https://doi.org/10.1007/s41748-025-00585-3

ORIGINAL ARTICLE

Determining Robust Optimal Pumping Solutions in a Heterogeneous Coastal Aquifer Using a Robust Decision-Making Approach and Bargaining Theory to Resolve Multiple Sources of Uncertainty

Ali Ranjbar[1] · **Claudia Cherubini**[2] · **Tom Baldock**[1]

Received: 24 June 2024 / Revised: 16 January 2025 / Accepted: 1 February 2025 / Published online: 21 February 2025
© The Author(s) 2025

Abstract

This paper analyses the impact of heterogeneity in the horizontal hydraulic conductivity field (K_{hf}) on the optimal pumping scenarios in a coastal aquifer and presents a multi-objective management framework to select robust optimal scenarios under high levels of uncertainty. Model speed is significantly improved by training an M5 Decision Tree (MDT) algorithm as a fast surrogate model for the density-dependent flow (DDF) in the SEAWAT code. The developed Tree model was linked to a non-dominated genetic algorithm (NSGAII) to determine Pareto optimal solutions, with the aim of maximizing total pumping volume and minimizing saltwater intrusion in a real case study, i.e., the Qom-Kahak aquifer, Iran. A linear sensitivity analysis explores the relationship between Pareto curves in response to variations in calibrated values of K_{hf} to quantify robust scenarios by a robust decision-making technique. Finally, the conflict resolution between minimum saltwater intrusion length, maximum pumping rate and robustness values is solved using a non-cooperative Nash bargaining theory. Results indicate that maintaining discharge from the pumping wells located far from 3 observation points in the case study, especially near the Salt Lake boundary, increases uncertainty in the Pareto solutions, where increasing K_{hf} by up to 30% of calibrated values induces a maximum 12% shift in the Pareto front for the scenario which led to high saltwater intrusion lengths. Moreover, the non-robust scenario causes the saltwater intrusion $\overline{SWI}$ zone to sharply advance to the area with a large number of pumping wells, while the scenario with high Nash product values led to a relatively uniform salinized zone which satisfies the allowed SWI length in 5 agricultural zones. In total, the developed MDT-NSGAII model is a computationally effective simulation–optimization model to find the Pareto front with 55 decision variables while achieving a 95% reduction in CPU time compared to the SEAWAT-NSGAII technique.

Keywords Saltwater intrusion · Robust decision-making · Pareto front · Surrogate model · Bargaining theory · Uncertainty analyses

Abbreviations

MDT	M5 decision Tree
DDF	Density-dependent flow
NSGAII	Non-dominated genetic algorithm
SWI	Saltwater intrusion
SMM	Surrogate meta-model
ANN	Artificial Neural Network
TDS	Total dissolved solid
SDF	Standard deviation reduction
RMSE	Root mean squared error
IGDT	Information-Gap decision-making technique
RDM	Robust decision making
GMS	Groundwater modeling system

✉ Claudia Cherubini
claudia.cherubini@units.it

Ali Ranjbar
a.ranjbarzeinalygharamaleki@uq.net.au

Tom Baldock
t.baldock@uq.edu.au

[1] School of Civil Engineering, University of Queensland, St Lucia, Qld 4072, Australia

[2] Department of Mathematics, Informatics and Geociences, University of Trieste, Via Weiss 2, 34100 Trieste, Italy

List of symbols

K_{hf}	Horizontal hydraulic conductivity field
K_c	Calibrated hydraulic conductivity
K_{cu}	Calibrated hydraulic conductivity of upper part
K_{cl}	Calibrated hydraulic conductivity of lower part
$\overline{SWI}$	Weighted average SWI wedge length
S/O	Simulation-optimization
S_s	Specific storage
n	Porosity
h	Groundwater head
C	Salinity concentration
t	Time
V	Velocity
ρ	Ground freshwater density
D	Dispersion vector
q	Pumping rate
R	Correlation coefficient
Ad	Aquifer width
r_c	Robustness threshold
$\overline{SWI}_{allowed}$	Allowed $\overline{SWI}$ length
a	Realization number
M	Nash product
Obj	Objective function

1 Introduction

Saltwater intrusion (SWI) is a significant challenge in coastal aquifers because of the increase in water abstraction for various uses. The transition zone between saltwater and freshwater is influenced by over-pumping, sea level rise, tidal effects, and climate change (Roy and Datta 2018). Consequently, the equilibrium between freshwater and saltwater is unstable and requires a management plan to control the SWI wedge under environmental threats.

Some previous studies have investigated the effect of future climate change and land use change on groundwater salinity which controls the management scenarios. Abd-Elaty et al., (2022) studied both recharge reductions associated with climate change and sea-level rise and concluded that sea-level rise causes a larger SWI length compared to recharge changes, in a hypothetical case study. In the same way, Imaz-Lamadrid et al., (2023) developed a climate change-oriented multi-parametric framework to assess the impact of climate change parameters on seawater intrusion in a coastal aquifer. To consider land use parameters as the sensitive parameter on SWI, Pisinaras et al. (2021) simulated aquifer salinization due to SWI intensified by land-use change and found that variability in aquifer recharge diminished aquifer freshwater reserves both in quality and quantity. Hussain et al. (2019) presented a review study for SWI management using physical subsurface barriers (land reclamation); the study showed that this technique effectively increases the freshwater body in coastal aquifers.

Further studies have focused on the sustainable management of polluted aquifers under pumping activities by means of simulation optimization (S/O) algorithms (Akter et al. 2024).

There are two approaches for modelling the SWI interface: sharp interface models and density-dependent flow (DDF) models. However, only DDF models are appropriate for SWI prediction in real-world case studies (Feist et al. 2022). Thus, the numerical solution based on the DDF model is linked to an optimization model to identify the optimum location and pumping rate of pumping wells under transient conditions (Werner 2017). However, the S/O process requires considerable computational time for the repetitive execution of the numerical code because of the updating of the groundwater head and salinity concentration as the key components for the optimization model (Uddin et al. 2023). Recent S/O studies have attempted to replace numerical solutions with an efficient surrogate meta-model (SMM) to reduce the computational times of S/O processes arising from a linkage between the SWI physical-based model and optimization algorithm (Secci et al. 2024). SMM techniques are single, or ensemble machine learning algorithms trained with samples of pumping and SWI rates, which are generated by finite difference or finite element numerical code (Yin et al. 2024). Because of the limitations of sharp interface theory and the CPU time of SWI numerical solutions, the S/O algorithm through the development of surrogate techniques has been introduced as the most popular method in recent SWI research (Jiang et al. 2021).

SMM methods for coastal aquifer management have been used over the past few decades. Secci et al., (2024) applied Artificial Neural Networks (ANN) as a surrogate model of DDF physical- based model to accelerate the CPU time of a S/O process during optimization. Kourakos and Christelis et al., (2023) indicated the capability of modular neural sub-networks for SWI management problems in a real case study which included a large number of pumping wells and boundary conditions. Roy et al., (2024) showed that genetic programming could predict SWI trade-off curves with less uncertainty and led to a 98% efficiency in CPU times when trained with the pattern of groundwater head and total dissolved solids (TDS) levels. In recent decades, different types of ANN models have widely used SMM techniques for real-world case studies (Shahabi, and Tahvildari 2024).

In particular, a range of nonlinear data-driven algorithms using different sampling methods have been well documented in surrogate modelling techniques, including Evolutionary Polynomial Regression (Mahboobi et al. 2023), the

Co-RBF algorithm (Durantin et al., 2017), Kernel Extreme Learning Machine (Song et al. 2018), Polynomial Chaos Expansion (Riva et al. 2015; Younes et al. 2020), Polynomial Response Surface (Yin and Tsai 2018), M5 tree and Random Subspaces model (Ranjbar et al. 2020) and Co-Kriging (Zhou et al., 2020, Christelis et al. 2023). In a review of the above-mentioned SMM techniques for SWI, Luo et al. (2023) concluded that no SMM algorithm is generally efficient, because the ability of each SMM varies for different problems and boundary conditions, such as head-controlled or flux-controlled systems. Furthermore, in the presence of complex boundary conditions and a large number of inputs, the accuracy of a single SMM may significantly decrease. Thus, an ensemble combination of many single SMMs, to use the capability of each model, can lead to a higher-accuracy SMM. Compared with single-data-driven surrogate algorithms, ensemble machine learning algorithms can provide high accuracy for unseen datasets (Jiang et al. 2021).

Li et al. (2022) implemented wavelet theory to reduce noise from observed data and increase the performance of the SMM for the prediction of salinity times series. Similarly, Wang et al. (2023) applied an Ensemble Kalman filter surrogate model, using a nonlinear ensemble of two different neural networks (ANN) for salinity prediction in a hypothetical aquifer. Their results indicated the high performance of the Kalman filter over a single ANN model for salinity contour predictions. Luo et al. (2023) compared the superiority and limitations of the data-driven SMM approach under different sampling methods for solute transport modelling. Their review highlighted the efficiency of local adaptive sampling methods in improving the performance of the SMM approach around the optimum point. Although deep learning SMM algorithms provide high prediction efficiency, they reduce the generality of SMM for unseen samples and hence lead to overfitting (Saad et al. 2023). Therefore, there is a trade-off between accuracy and the generality of ensemble and single SMM techniques. Moreover, for the same case study, the efficiency of different ensemble SMM techniques varied with the sampling method.

A review of surrogate models in SWI management studies indicates that many surrogate models attempt to accelerate the S/O process and increase prediction accuracy by using different machine learning and sampling methods. The aim of these surrogate models is to develop a computationally efficient prediction model to link with the optimization model and identify the Pareto-optimal solution while avoiding a local optima trap. However, the uncertainty in the calibrated parameters on Pareto optimal scenarios has rarely been analyzed in SMM approaches. Several studies have investigated the effect of heterogeneity in calibrated hydraulic conductivity on SWI using different Monte Carlo realizations and the spatial correlation of hydraulic conductivity (Pool et al. 2015; Houben et al. 2018). Nevertheless, a comparative analysis between Pareto objectives and their uncertainty in multi-objective problems remains a challenge for decision-making purposes. Thus, the uncertainty in aquifer parameters, such as inherent heterogeneities and the hydraulic conductivity field must be linked to management scenarios that are obtained from Pareto solutions. Regarding the complex relationship between the heterogeneity of an aquifer and SWI length, an accurate evaluation of the uncertainty effect on the scenarios of the Pareto front requires a computationally efficient management framework (Ketabchi and Jahangiri, 2021).

In this study, a novel decision-making algorithm is developed for the management of coastal aquifers to determine the Pareto curve under uncertainty in the hydraulic parameters of the aquifer. To find the Pareto front in this study, a surrogate-based S/O model was developed and linked to the SEAWAT model based on the DDF assumption. The proposed surrogate model and optimization algorithm is a machine-learning approach based on the M5 tree and NSGAII algorithms. A clustering-based model was developed to reduce the number of inputs corresponding to the pumping rates in a real case study that included a large number of pumping wells. The sensitivity of the Pareto curve to aquifer hydraulic parameters was examined by applying different realizations of the horizontal hydraulic conductivity field (K_{hf}). The dataset obtained from a sensitivity analysis was used for the uncertainty assessment of different pumping scenarios based on the information-gap theory and to quantify the robustness of the pumping scenarios. Finally, we select the most desirable pumping scenarios from the Pareto curve solution using Nash conflict resolution theory for decision-making purposes.

2 Materials and Methods

The methodology proposed in this study is based on training a computationally effective SMM for the prediction of salinity time series with the response of the SEAWAT model to different pumping strategies and general head boundary conditions. The SEAWAT model was then replaced with the SMM and linked to an optimization model to investigate the most robust optimal scenarios due to uncertainty in K_{hf} of a heterogeneous aquifer. A flowchart of the proposed surrogate-based decision-making approach is shown in Fig. 1.

As demonstrated in Fig. 1, the first objective of this study is coupling the fluid flow MODFLOW and solute transport MT3DMS code in the density-dependent SEAWAT model, to simulate a time-variant SWI wedge under the DDF assumption. The developed SEAWAT model is then

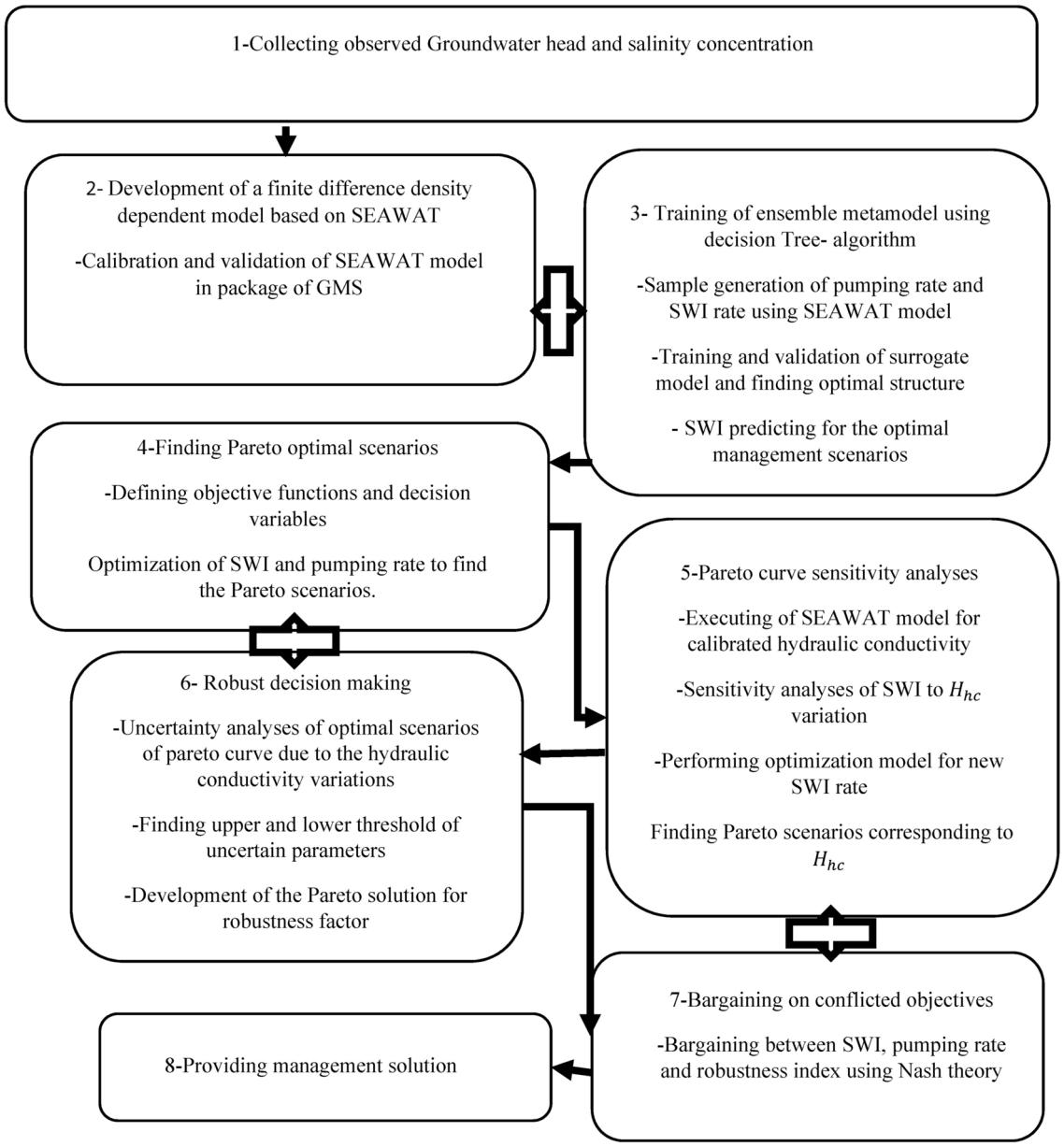

Fig. 1 The flowchart of the proposed surrogate decision-making model incorporating uncertainty

replaced with an M5 decision tree (MDT) based surrogate model to reduce the computational time of the S/O process for the Qom-Kahak aquifer incorporating a large number of pumping wells and two types of boundary conditions. The second objective is identifying the Pareto optimal pumping volume under minimum saltwater intrusion after the MDT model was trained with the key parameters of the SWI in the form of input–output and linked to the NSGAII optimization model. To avoid local optimum traps, the MDT was verified and sampled using the adaptive method with newly generated samples by the SEAWAT model. The third objective was the development of a linear sensitivity analysis model to assess the influence of heterogeneous variations in K_{hf} on the SWI wedge. Therefore, the robust Pareto scenarios under these sensitivity results are identified and applied for uncertainty assessment by the robust management approach based on the Information-Gap decision theory (IGDT) method. Finally, Nash bargaining theory is applied to solve the conflict between the Pareto solution components and to find the most preferred scenarios.

2.1 Brief Description of the SEAWAT Module

The SEAWAT model (Guo and Langevin 2002) is a finite-difference code based on the variable-density flow assumption for modelling SWI by coupling MODFLOW

for groundwater flow modeling (McDonald 1988) with MT3DMS for solute transport modelling (Langevin and Guo 2005). The main parameters of the SEAWAT engine utilized in this study were the initial head and TDS values at the Salt Lake Boundary (Qom aquifer), head and TDS observation points, temporal and spatial recharge rates, aquifer geology and conductivity, river and drain stages, and conductance.

The main parameters used to calculate groundwater head and salinity contours based on the finite difference solution in this study include Hydraulic conductivity (K), specific storage(S_s), porosity (n), groundwater head (h), salinity concentration (C), time (t), density of saltwater water (ρ_0) generated by the sink or source, ground freshwater density (ρ), hydrodynamic dispersion vector (D), and leakage velocity parameter (V). To simulate the SWI in the framework of sustainable operation under uncertainty in horizontal hydraulic conductivity, SEAWAT was applied in GMS. 10 *packages* as shown in Fig. 2.

2.2 Brief Description of the Surrogate Model

In traditional machine learning models such as neural networks and regression models, there is a black box relationship between the input and output variables (Shehab et al. 2023). However, some machine learning algorithms, such as M5 decision tree (MDT) models, generate multiple linear and nonlinear relations between the input and output patterns, which indicate the sensitivity of the output parameters to the input parameters (Forrester et al. 2021). In the MDT method, nonlinear equations are split into several simple regression relations. Therefore, an MDT provides regression relations to predict nonlinear problems such as flow and solute transport equations (Li et al. 2022).

MDT uses the standard deviation reduction (SDR) factor to partition the feature space into leaves and nodes and then assigns a regression equation to each leaf as defined below (Frank et al. 1998):

$$SDR = K(F) - \sum_i \frac{|F_i|}{|F|} \times K(F_i) \quad (1)$$

where F represents samples devoted to node i. F_i are the generated samples after splitting the node i, and K shows the standard deviation factor. When the SDR satisfies the threshold values, the MDT decides to stop creating a new node, and the generated relationships in the leaves are utilized for the prediction step. The reason for stopping the generation of new nodes is that the prediction accuracy cannot increase by increasing new nodes; hence, growing a big tree result in overfitting for local samples (Alnahit et al. 2022).

In this study, we used the exponential form of a quadratic function to create a nonlinear regression for each range of $\overline{SWI}$ under different pumping rates as follows:

$$\overline{SWI}(q) = \sum_{i=1}^{n} x_1 + x_1.(q_1)^{f_1} + \ldots + x_i.(q_k)^{f_i} \quad (2)$$

where f_i and x_i are constant coefficients obtained by trial and error for each node and leaf, q_k are extraction rates from the kth well and $\overline{SWI}$ represents saltwater intrusion.

2.2.1 Brief Description of the M5 Decision Tree Model Considering Uncertainty

For a large number of inputs (pumping wells), as in the case study, the development of a single MDT model is excessively time-consuming. Thus, the input space was divided into several small parts, and a single MDT model was fitted to each part. The predicted value from a single MDT model was used to develop a comprehensive MDT model. Therefore, instead of training a single complex tree for a

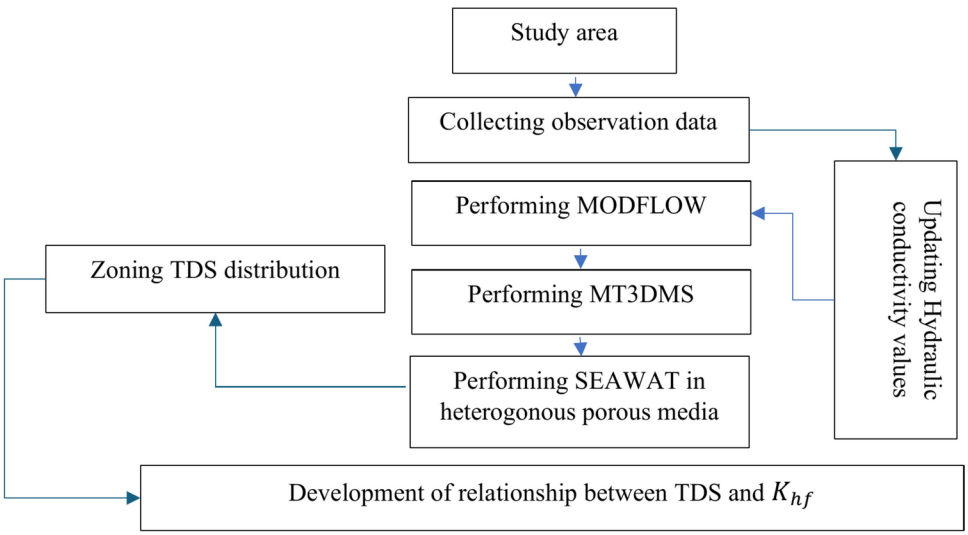

Fig. 2 The proposed steps for the SEAWAT model in this study

large number of inputs, many efficient MDTs were defined as a small number of outputs. In this regard, an effective approach is to divide the input area into many circular parts to understand the sensitivity of each input (55 pumping wells) to a single output (3 observation wells). This concept assumes that the salinity level and groundwater head are considerably affected by discharge from adjacent operational wells (Kourakos and Mantoglou 2009). Therefore, wells inside the circular area were ranked using sensitivity analyses of two factors: the distance from the observation well and the total pumping volume. The ranking values ($R_{i,j}$) for the pumping wells (w_i) and observation wells (Obs_j) are described as follows:

$$R\left(i,j\right)=\left(c_{1,1}c_{1,2}\ldots c_{i,j}\right) \tag{3}$$

The circular area is updated during the learning process using new samples generated by the SEAWAT numerical model. The performance of the MDT model is evaluated using the statistical criteria index as below:

$$R^2=\frac{M_0-M}{M_0} \tag{4}$$

$$M_0=\sum_i\left(O_{SEAWAT}-\overline{O}_{\mathrm{MDT}}\right)^2 \tag{5}$$

$$M=\sum_i\left(O_{SEAWAT}-\widehat{O}_{\mathrm{MDT}}\right)^2 \tag{6}$$

$$\widehat{O}_{\mathrm{MDT}}=\left(\sum_{i=1}^{n}X_{SEAWAT}\right)/n \tag{7}$$

where O_{SEAWAT} is calculated by the numerical model, $\overline{O}_{\mathrm{MDT}}$ is the predicted value of the MDT model, and $\widehat{O}_{\mathrm{MDT}}$ is the average value of n samples simulated by MDT. Moreover, the minimum mean absolute error (MAE) and the root mean squared error (RMSE) are used as a discrepancy criterion of the prediction model:

$$MAE=\frac{1}{n}\sum_{i=1}^{n}(O_{SEAWAT}-O_{MDT}) \tag{8}$$

$$RMSE=\left[\frac{1}{n}\sum_{i=1}^{n}(O_{SEAWAT}-O_{MDT})\right]^{\frac{1}{2}} \tag{9}$$

2.2.2 Sampling Method

In this study, an optimal Latin hypercube sampling method (OLHSM) was used to independently generate samples throughout the whole decision area (Qiang et al. 2024). The minimum distance between samples (pumping rate of 55 wells) was increased by assigning the same weight and intervals to each well and then samples were simulated in MODFLOW and SEAWAT to obtain groundwater heads (h) and TDS concentrations, respectively. To reduce the dimensions of the samples, we used the K-means clustering algorithm developed by Ranjbar and Mahjouri (2020) for the Qom Kahak aquifer. The center and diameter of the circular sampling area change adaptively based on the predicted variance as follows:

$$Snew_i=\arg maximum\,\alpha\left(S_i\right)\left(S\mathcal{E}A\right) \tag{10}$$

where A is the sampling area, α represents the predicted variance and S_i indicates the number of samples. A uniform distribution of the 55 pumping rates have in the five clustered zones was assumed. To avoid training the MDT model over local samples that cannot cover the entire learning space, all 5 pumping zones were discretized at 100 m^3/day intervals (approximately 1.5% of the maximum pumping rate) and then reduced to 20 m^3/day during the training stage.
The total number of initial samples considering 5 clusters with 100 m^3/day intervals and a maximum pumping rate of 6400 m^3/day was considered. The first 320 samples were generated by the SEAWAT model and then extra samples (30% of initial samples) were generated based on the efficiency of the MDT model. In each sampling iteration, the $\overline{SWI}$ simulated by SEAWAT and mean standard deviation error (MSDE) of TDS in the observation wells were recorded. The sampling process was maintained until the MSDE converged to 5 mg/l. It is noteworthy that the efficiency of the aforementioned sampling approach is principally applicable to this case study and needs to be improved for other case studies.

2.3 Optimization Model

The optimization algorithm developed for the Qom-Kahak aquifer groundwater includes a large number of production wells. The multi-objective optimization algorithm is composed of two conflicting objectives: maximization of the total extraction rate and minimization of the $\overline{SWI}$ length. The criterion for the $\overline{SWI}$ length in this study is the area of the agricultural zone polluted by saltwater intrusion (iso line TDS 75%). To obtain the Pareto curve between the two objectives, a Non-dominated Sorted Genetic Algorithm-II (NSGAII) (Deb 2002) was implemented. In the last decade,

many different improvements have been made to NSGAII through optimization selection, crossover, and mutation parameters. In this study, we conducted an optimized form of the NSGAII, which is a high-dimensional multi-objective algorithm presented by Fan et al. (2024). The S/O process is first coupled with the SEAWAT model to formulate the structure of the S/O algorithm for the NSGAII-MDT combination, This was performed to verify the accuracy of the samples predicted by the SEAWAT model. An adaptive flowchart of the coupled S/O and MDT models is shown in Fig. 3.

The proposed SWI management algorithm for maximizing the total water extracted over the operation period can be mathematically stated as follows:

$$Maximize f(Q) = \left(\sum_{i=1}^{n} \left[\left(\sum_{t=1}^{T} Q_{i,t}.\Delta t \right) \right] \right) \tag{11}$$

subject to

$$\overline{SWI_t} = g(Q) \tag{12}$$

$$\overline{SWI_t} < \overline{SWI_{max}} \; and \; Q_{min} < Q_{i,t} < Q_{max} \tag{13}$$

where f is the total extracted water from the pumping wells, $Q_{i,t}$ refers to the pumping rate at the time step t and ith pumping well, n represents the total number of pumping wells, g is a function of the DDF equations simulated by the SEAWAT model, Q_{min} and Q_{max} are the minimum and maximum permissible pumping rate which are considered to be 150 m^3/day and $6450m^3/day$, respectively.
$\overline{SWI}$ is the weighted average SWI zone length calculated as follows:

$$\overline{SWI} = \frac{L(TDS_{T=t}(75\%)) - L(TDS_{t=0}(10\%))}{Ad} \tag{14}$$

and where $L(TDS_{t=T}(75\%))$ and $L(TDS_{t=0}(10\%))$ are the distance of 75% and 10% TDS contours from the salt Lake boundary respectively, which are considered 7500 $\frac{mg}{lit}$ and 1100 $\frac{mg}{lit}$ respectively, $Ad = 8200m$ is the aquifer width near Salt Lake boundary.

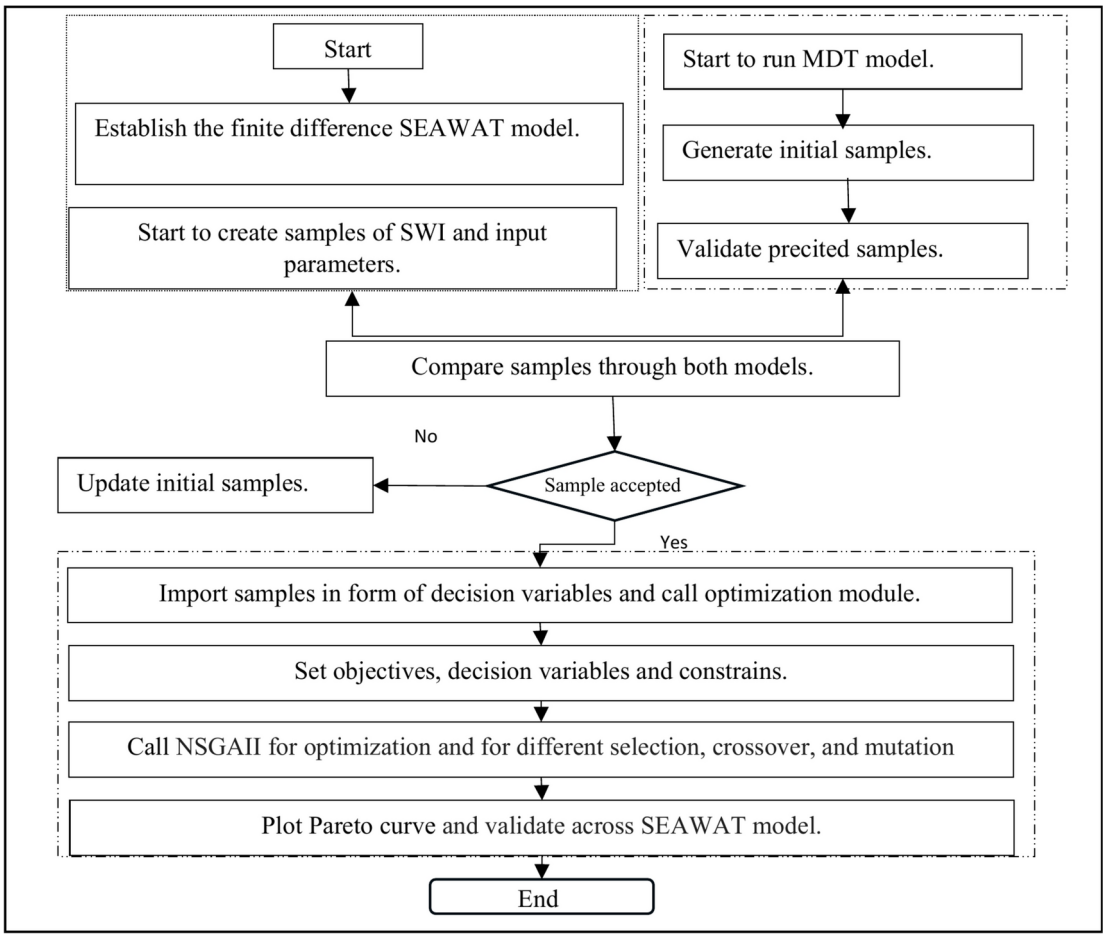

Fig. 3 Workflow of the integrated S/O model and MDT model

2.4 Robust Decision Making

In the present study, an Information-Gap decision-making technique (IGDT) was used to maximize the robustness of the optimal scenarios when there is uncertainty in K_{hf}. Based on the observational data, the lower and upper bounds of each sensitive and uncertain parameter were determined and discretized around the average value. Regarding the n different value of K_{hf} associated to n observation points, K_{hf} was divided into *m* intervals. Thus, there are $m+n$ cases of K_{hf} realizations for uncertainty assessment and hence the SEAWAT model is performed $m+n$ times to assess all possible cases. In IGDT, the robustness of an optimal scenario is defined as the maximum variation of a parameter around the average value when the objective function exceeds a robustness threshold (r_c). The robustness threshold is a percentage of the objective function which is determined by engineering judgment. To find r_c in this study, the SEAWAT model has been performed for different realizations of K_{hf} around the calibrated value. The robustness thresholds are defined as follows:

$$r_{c,j} = obj_{i,max} - fi \times \left(obj_{i,max} - obj_{i,min}\right) \tag{15}$$

where $r_{c,j}$ are the robustness thresholds for the scenario j, fi is a coefficient that varies from 0 to 1, and $obj_{i,max}$ *and* $obj_{i,min}$ are the maximum and minimum values of the objective function, respectively.

In the present study, to implement IGDT and assess the uncertainty of management scenarios related to the hydrogeologic parameters of the aquifer, a robustness value was defined for each management scenario. The $\overline{SWI}$ values are recorded for different realizations from $a = 1, 2, \ldots N$, where a is the realization number and N is the total number of realizations. The maximum value of the parameter a for the scenario i (n_i) which satisfies the allowed $\overline{SWI}$ length ($\overline{SWI}_{\text{allowed}}$) under the allowed pumping volume, is considered as the robustness of that scenario as defined below (Ghodsi et al. 2016):

$$n_i = \max(a : (SWI)_i < \overline{SWI}_{\text{allowed}}) \quad a = 1,2,3\ldots,N \tag{16}$$

2.5 Bargaining Using the Nash Theory

The Nash bargaining approach (Nash, 1950) is based on stakeholders' utility functions to choose the best scenario, with the Nash product defined by:

Maximize

$$M = (p_1 - Obj_1)^{W_1} \times (p_2 - Obj_2)^{W_2} \times \ldots.. \times (p_J - Obj_J)^{W_J} \tag{17}$$

S.t: $Obj_k < Obj_k \quad k = 1, \ldots, J$

where M is Nash product factor, Obj_k is the objective function of stakeholder *k*, p_k is the value of optimal scenarios attributed to each stakeholder *k*, W_k is the strength of stakeholder *k*. The best scenarios among the Pareto optimal scenarios have a maximum value of M.

3 Case Study

To evaluate the performance of the proposed methodology, the sustainable management of the Qom-Kahak aquifer was assessed. The study area (34°15'34°45'N;50°,45'51°,30'E) is located in the southern part of Qom City, Iran (Fig. 4). The Lake boundary in the southern part of the aquifer causes saltwater advancement into the 122 km^2 of agricultural and domestic zones. The boundary condition of the aquifer is a specified head from the Lake boundary in the south and a general head boundary condition in the west and north. The study of the geological formations of the aquifer indicates an alluvial structure with heterogeneous hydraulic conductivity between $1.2m/day$ and $54m/day$ in the southern and western sections, respectively, which is the main source of uncertainty in the calibration stage. The mean recharge rate through the aquifer varies from 0.06 to 0. 07 mm/day . Regarding the low elevation of the southern part adjacent to Salt Lake, the SWI is impacted by 55 pumping wells in this part while the other pumping wells (780 wells) have negligible effect on the SWI. Figure 4 shows the location of pumping wells, polluted wells near Salt Lake, and observation points. The maximum observed groundwater level is 898 m near Qom City River (Ranjbar et al. 2020).

Moreover, the transient variation of discharge rate for a stress period of 4 years is listed in Table 1. These agricultural wells are located near the Salt Lake boundary and significantly affect SWI wedge advancement to the aquifer. Fifty-five pumping wells and 3 observation wells are located in the unconfined part of the aquifer, and their information is implemented for numerical modeling in this study (Table 1). Ninety percent of well screens are at a depth between 15 m to 45 m under ground surface.

4 Results and Discussion

4.1 Numerical Simulation

The management zone (see Fig. 5) with a dimension of 15 km (length) × 8 km (width) is divided into 500 m × 500 m mesh cells and two geological layers. A simulation period of four years is discretized into 48 monthly time steps. The initial TDS level at the Lake boundary based on observation

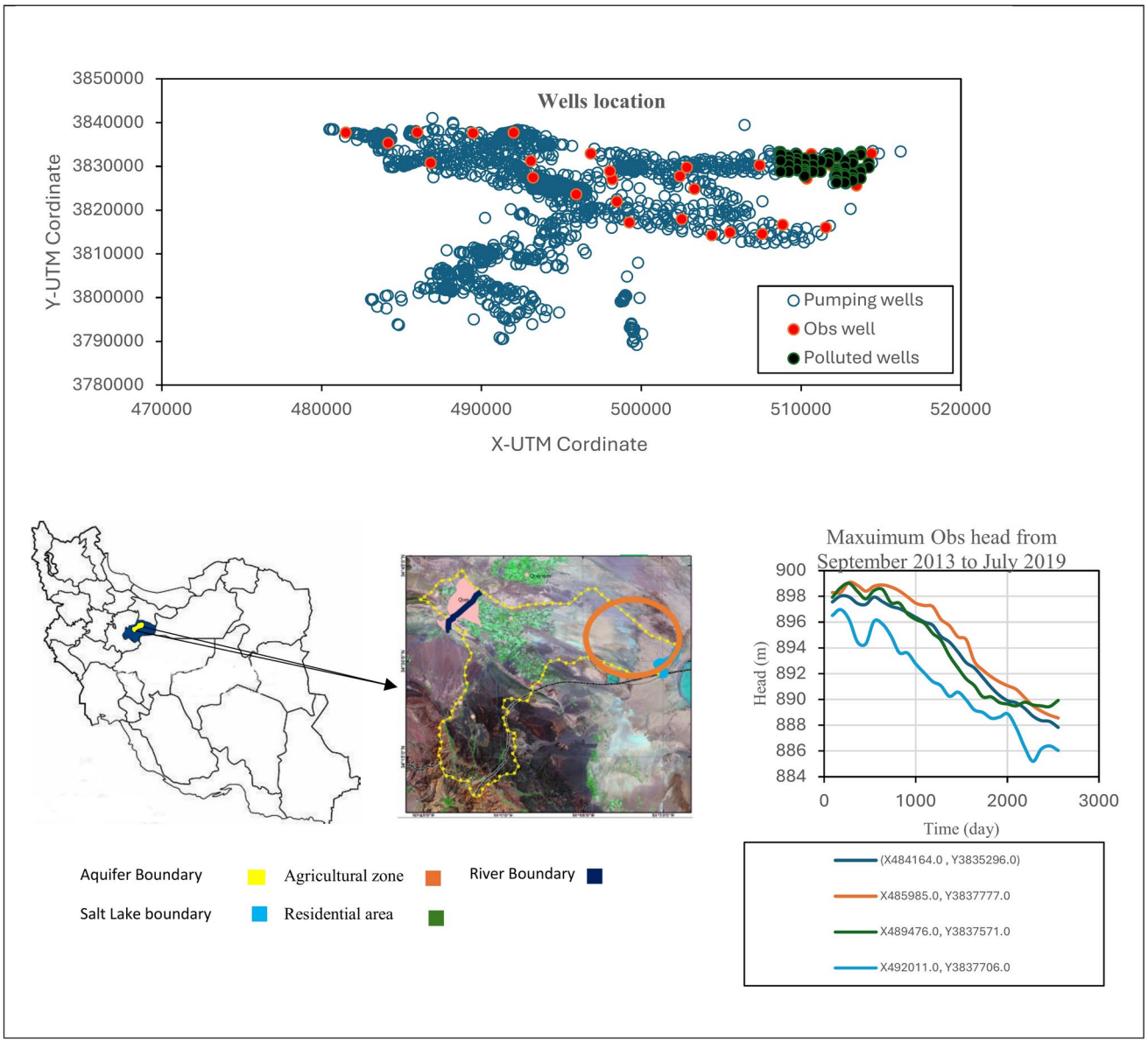

Fig. 4 The main characterization of the Qom-Kahak aquifer such as pumping observation wells coordination, and aquifer land use (the source is MODIS records)

data was considered 12. 5 (gr/l). To simulate the head level near the Lake boundary, a time variant specific head from 8 to 12 m was applied in the MODFLOW module of SEAWAT. The 3rd order total variation diminishing (TVD) numerical plan wass applied to solve the advection and dispersion equation for the salinity level in the MT3DMS module of SEAWAT. Similarly, the groundwater head model was calibrated across coefficients of hydraulic conductivity in the transient comedian to reduce the mean absolute error (MAE) and Root mean square error (RMSE) between observed and simulated groundwater heads in 2 observation wells of the total 24 wells thorough the aquifer (4 wells located in the management zone). Results indicate an acceptable range of error indexes between 1.5 m and 1.8 m for 3 observation points near the Lake boundary at the end of simulation period (2462 days).

Table 2 presents the initial values of the TDS and Chlorine ion concentrations, recorded at 18 observation points. The minimum and maximum values of Chlorine ion concentration through the aquifer are 63 (mg/l) and 4100 (mg/l), respectively, while the TDS concentration varies between 500 (mg/l) and 11,700 (mg/l), respectively. There is good agreement between the Cl and TDS levels at 18 observation points (see Fig. S4) and hence, TDS concentration was considered the salinity indicator.

Table 1 A summary of groundwater pumping rates (m^3/day) information and coordination near the Salt Lake

X (m)	Y (m)	Q (T=272)	Q (T=637)	Q (T=1002)	Q (T=1367)	Q (T=1732)	Q (T=2097)	Q (T=2462)
514,219	3,830,768	916	902	1036	1036	916	902	1036
514,219	3,829,768	1026	974	1484	1483	1026	974	1483
513,719	3,833,268	697	661	1007	1007	697	661	1007
513,719	3,832,768	882	837	1275	1274	882	837	1275
513,719	3,829,268	882	837	1275	1274	882	837	1275
513,719	3,828,768	787	773	484	435	787	773	484
513,719	3,827,268	716	702	836	836	716	702	836
513,219	3,832,268	888	871	1037	1036	888	871	1037
513,219	3,831,768	1401	1404	1234	1218	1400	1404	1234
513,219	3,830,768	501	492	585	585	501	492	585
513,219	3,828,268	510	625	836	713	510	625	836
513,219	3,827,268	1422	1350	2056	2056	1422	1350	2056
513,219	3,826,768	215	211	251	251	215	211	251
512,719	3,831,268	591	579	690	689	591	579	690
512,719	3,828,268	978	938	1324	1324	978	938	1324
512,719	3,827,768	86	84	100	100	86	84	100

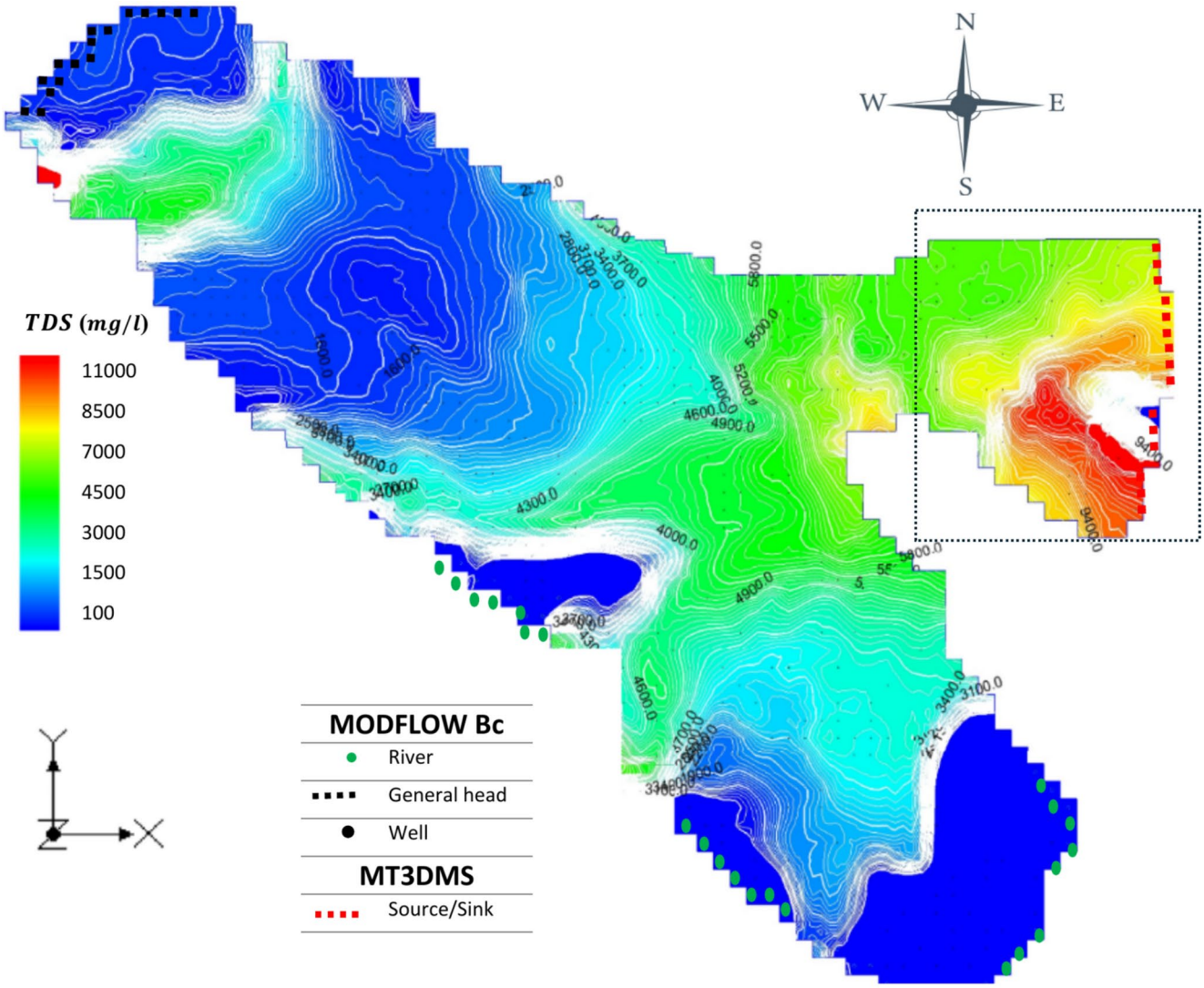

Fig. 5 The map of salinity contours for the study area, the distribution of the concentration of the total dissolved solids (TDS), the location of the current observation and pumping wells, and the total groundwater pumping rate in the five agricultural zones

Table 2 The initial values of TDS and Chlorine ion concentrations of 18 observation points

Obs point	UTM-X	UTM-Y	TDS (mg/l)	CL (mg/l)
K5	3,835,869	483,926	6316	2029
K29	3,836,428	491,277	5598	1612
K34	3,826,444	492,517	3925	984
K35	3,830,983	492,641	2864	846
K46	3,826,013	496,942	5811	1717
K49	3,820,800	498,295	5832	1682
K50	3,830,150	498,559	3905	1275
K53	3,819,769	501,367	2014	422
K55	3,826,171	501,683	6279	2004
K56	3,816,846	501,818	846	140
K58	3,820,557	502,344	3448	946
K63	3,828,758	505,247	8415	2958
K65	3,830,339	506,151	6269	2103
K67	3,819,804	506,485	3977	1331
K72	3,813,813	508,872	1865	389
K74	3,831,622	510,283	6674	2218
K75	3,828,871	511,146	7695	2814
K77	3,827,390	513,516	11,129	3792

Table 3 Aquifer parameters used for MT3DMS and MODFLOW

Parameter	Lower part	Upper part	Units
General head conductance	3529	260,992	m^2/day
Recharge	0. 0635	0. 0779	mm/day
River conductance	2	5050	m^2/day
River stage	0	903	m
Specified head	809.35	811.56	m
Pumping rate	0	5600	m^3/day
TDS	120	12,600	mg/lit
Hydraulic conductivity	1.2	54	m/day
Specified storage	0.03	0.06	%
Longitudinal dispersivity	3	8	m
The ratio of horizontal transverse dispersivity to longitudinal dispersivity	1	1	-
The ratio of vertical transverse dispersivity to longitudinal dispersivity	0.1		-

The transient movement of the saltwater wedge into the Qom-Kahak aquifer was studied by simulating the polluted area using the SEAWAT module in GMS. 10 package.

Figure 5 illustrates the SWI advancement (corresponding to a 75% Iso line TDS concentration) of 5 km to the northern part of the aquifer, which is surrounded by agricultural lands.

The red line represents the maximum TDS concentration which indicates the presence of saltwater intrusion. Approximately 35 km^2 of farmland near the Salt Lake is threatened by a high volume of saltwater entering the aquifer. The ranges of the aquifer hydraulic and solute transport parameters are presented in Table 3.

4.2 Development of an Efficient Surrogate Algorithm

In this section, the model performance is examined by identifying the transient discharge rates and heads during 6 years of pumping activity. To examine the efficiency of the MDT model as an SMM, the generated samples were verified using the hold-out approach and thus 33% of the total samples were used for verification. The performance of the surrogate model was examined by measuring the root mean squared error (RMSE), the mean absolute error (MAE), and the correlation coefficient (R^2) between the corresponding point values in the SEAWAT model and the surrogate model.

Figure 6a and c demonstrate a comparison of the predicted TDS concentration and those from the SEAWAT model on the 1700 training data from 5300 samples (indicated by the red point) at the beginning and end of the stress period, respectively. The predicted value of the MDT in the validation stage (Fig. 6b and d) confirms that the surrogate model fits the training data well and has a strong performance in the prediction of the density-dependent flow model with the lowest error ($< 150mg/l$) and a high correlation coefficient (>0.97). The predicted TDS concentration values are interpolated over the observation points to quantify SWI (Fig. 6e and f). Figure 6e and f, indicate that the predicted values of the MDT model for $\overline{SWI}$ ($\Delta t = 30$) are in good agreement with those simulated by the SEAWAT model. As demonstrated in Fig. 6f, the MDT model performs with high accuracy for predicting $\overline{SWI}$ in both the calibration and verification stages.

The statistical criteria of the $\overline{SWI}$ length predicted by the MDT model for $\Delta t = 30$ days ($\Delta\overline{SWI}$) corresponding to different pumping rats are is presented in Table 3. In summary, Table 4 shows that the RMSE values of TDS and head for the testing samples are less than 1% of the maximum values, and thus the MDT results are in good agreement with the SEAWAT model.

However, due to the repetitive process of the MDT, where time t is utilized to predict time $t+1$, the total error is aggregated and hence caused an increase in RMSE and a reduction in correlation coefficient values. Although the MAE value for the groundwater head is slightly high for the testing samples, the overall head value is overestimated by the MDT model and hence, the model predictions are conservative for decision-making purposes.

The TDS concentration, $RMSE$ and R values for the training and validation steps are significantly similar. These results indicate that the proposed MDT model can effectively simulate highly nonlinear variation in SWI length, regardless of the uncertain parameters.

The observed salinity data (TDS concentration) are recorded in a monthly time step for one year before the

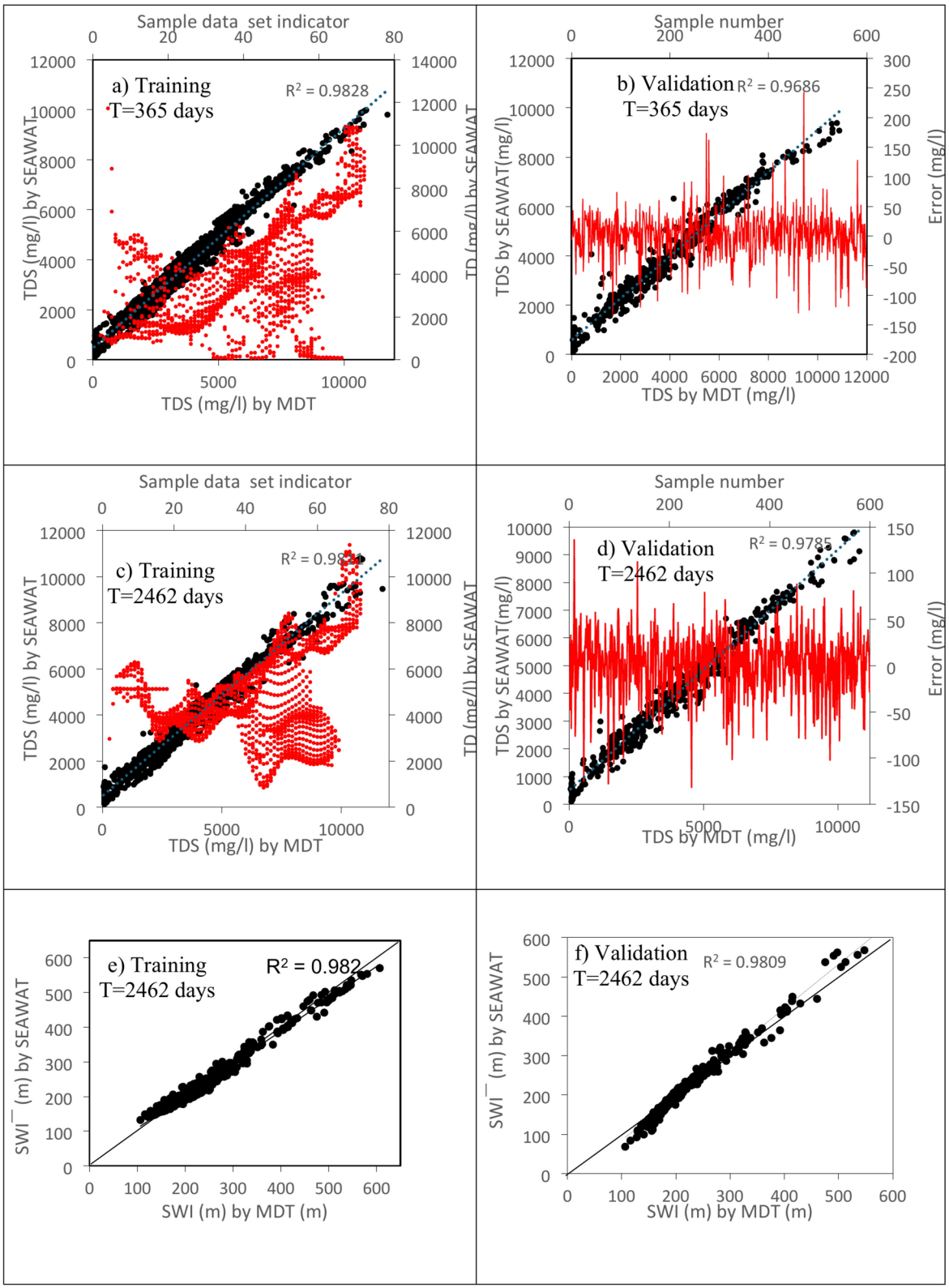

Fig. 6 Scatter plots of simulated TDS and associated SWI by SEAWAT versus MDT model during the simulation period for both calibration and verification stage

Table 4 The minimum and maximum values of the predicted Heads and TDS over observation points for T=273 days

Samples	Min	Max	Mean	Median	St
$Head(m)$	802.06	906.58	854.38	853.38	32.27
$TDS(mg/lit)$	850.91	11,370.58	4743.93	4303.98	1848.47
$\overline{SWI}(m)$	2550	5200	-	-	-
Predicted training		R	RMSE	MAE	
$Head(m)$		94–97%	18.25	39.30	-
$TDS(mg/lit)$		95–98%	145.51	180.45	-
$\overline{SWI}(m)$		95–98%	65.25	81.43	-
Predicted validation		R	RMSE	MAE	
$Head(m)$		93–96%	20.53	40.12	-
$TDS(mg/lit)$		92–96%	180.26	192.24	-
$\overline{SWI}(m)$		92–96%	70.87	85.32	-

Table 5 The details of decision variables and NSGAII parameters

Zone ID	1	2	3	4	5
Land use	Wheat and Maize	Maize	Orchards	Cotton and wheat	Chery tree
Wells	26	21	5	10	14
Q rate (m^3/day)	61,000	5885	23,100	5650	12,450
generations	evaluations	population	points	Objectives	generations
320	1450	240	28	2	320

operation horizon (6 years). Salinity data from 3 observation wells near Salt Lake (k74, k75 and k77) are used to calibrate the SEAWAT model parameters. The graph of the simulated TDS by SEAWAT m and MDT model versus the observed values at Observation well k77 is illustrated in Fig. S5. As seen, the RMSE value of the predicted TDS (250 mg/l) by SEAWAT and MDT for validation step is less than 2 % of the maximum TDS values (12500 mg/l), and thus the MDT results are in good agreement with the observed values.

4.3 Optimization

The NSGAII algorithm was coupled with the MDT model to investigate the optimal trade-off curve between $\overline{SWI}$ and profit over a 6-year horizon period. The profit is defined as a function of the extraction rate (55 wells are active) and land use type (Table 5). Thus, there are 6x4x55 decision variables associated with 55 extraction wells over 6 years, with a 3-month step. The MDT model is updated during the optimization process using the SEAWAT model samples to reduce learning space related to the pumping rate of different wells,. Therefore, if the RMSE for a sample is greater than the threshold (35 mg/l), the sample is removed from the data set. In this study, the MDT model was adaptively retrained 28 times with the SEAWAT model to satisfy the *RMSE* threshold, and then the initial samples (260) were generated. NSGAII is performed to find a trade-off curve between the two objectives associated with different structures of NSGAII parameters (provided in Table 5).

NSGA-II identified Pareto front from 20 uniform random start points with 100 iterations.

Figure 7a shows the net saltwater intrusion area for different extraction strategies from 5 agricultural zones (55 wells). It can be seen that the minimum $\overline{SWI}$ ($1.35km$) corresponds to zero extraction rate, although the MDT overestimates $\overline{SWI}$ length in the scenarios with low pumping rates. However, there is good agreement for the middle part of the Pareto curve with the current pumping rates.

A comparison between the SEAWAT-NSGAII and MDT-NSGAII models confirms that there is a small error and good correlation. Because the clustered wells inside the Qm zone are located near the Salt Lake boundary, pumping from this zone has a significant effect on left-hand side of the Pareto curve, where the SWI wedge covers this zone ($\overline{SWI} < 1.8km$). Although pumping from the wells located in $Q4$ increases $\overline{SWI}$ length, their impact on a small value of $\overline{SWI}$ length is negligible. The result in Fig. 7b indicates that wells inside $Q5$ and $Q4$ zone control the SWI wedge and shape.

Although, there is a small error in the predicted $\overline{SWI}$ length between MDT-NSGAII and SEAWAT-NSGAII however, the run time has been reduced considerably by applying MDT-NSGAII. The computational time for each SEAWAT run and training MDT algorithm is approximately 2 min and 2.3 min, respectively which results in a run time of approximately 45 min for MDT-NSGAII whereas, the total CPU time of the linked SEAWAT-NSGAII model is approximately 12 h. The NSGAII parameters are presented in Table 4, the total required time of the MDT-NSGAII algorithm is approximately 5% of the SEAWAT-NSGAII model. The Pareto results provided in Fig. 7a and b incorporate calibrated parameters for the aquifer properties and thus the robustness of these scenarios to aquifer parameters, e.g., K_{hf}, are assessed in the next section.

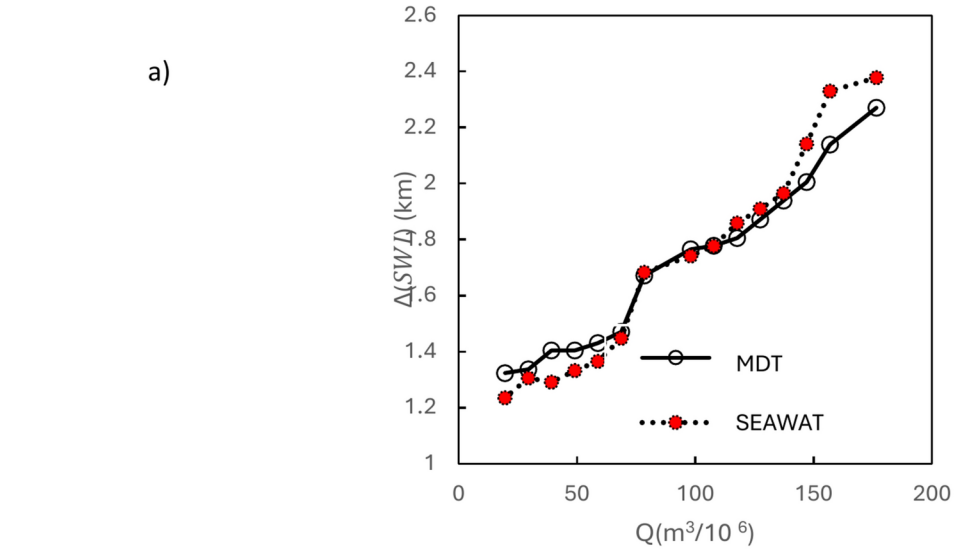

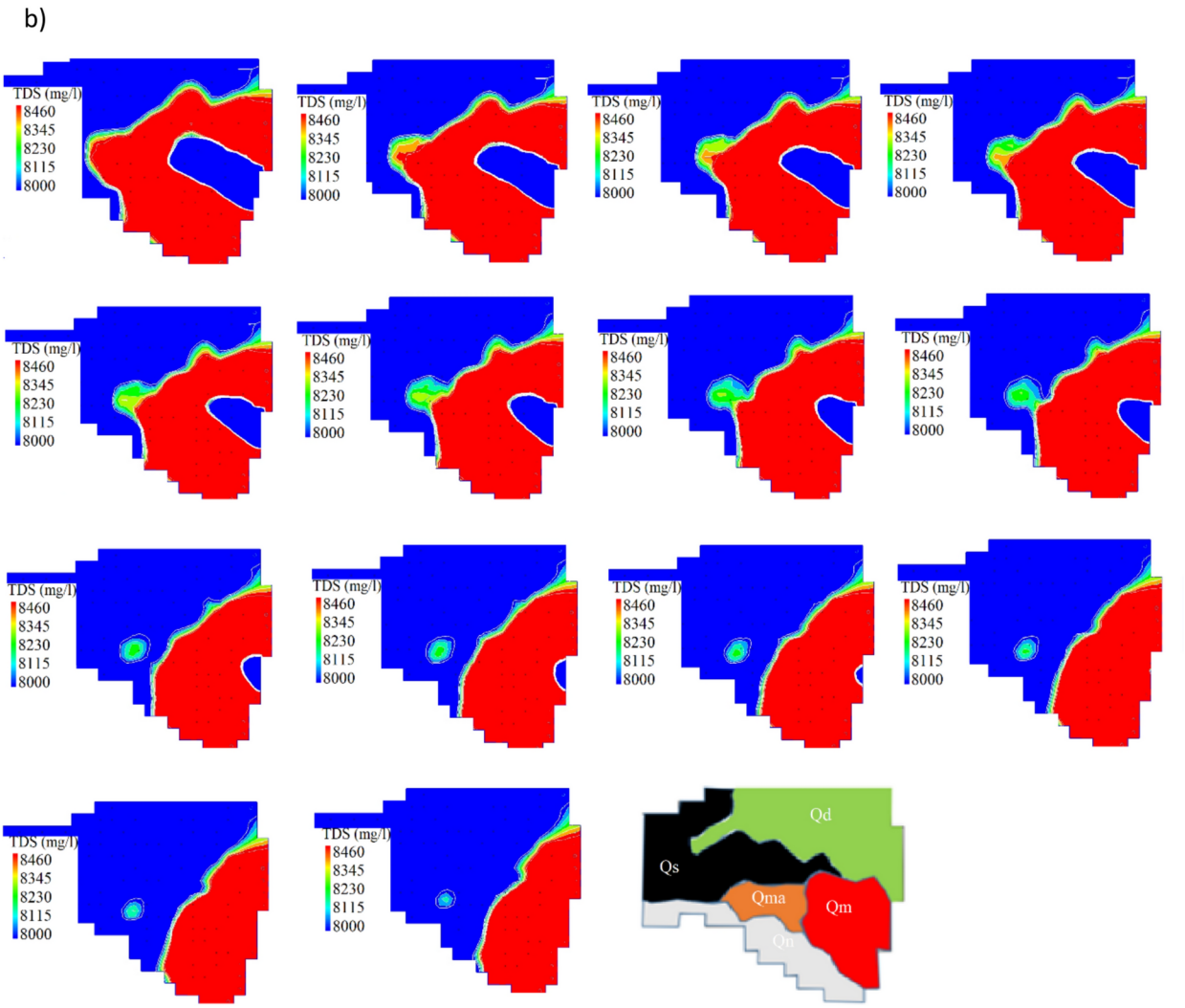

Fig. 7 The saltwater wedge movement in different part of aquifer for the Pareto scenarios a) the trade-off curve predicted by MDT-NSGAII versus simulated by SEAWAT-NSGAII for 6-year operation period b) The final shape of SWI wedge for Pareto optimal scenarios for a time period of 2462 days. $(Q_{ma}, Q_d, Q_n, Q_m, Q_s)$ are pumping rate from wells located in the Malekan, Dolatabad, Noran, Momenabad and Serajeh agricultural zone, respectively)

4.4 Uncertainty Assessment on the Pareto Curve

4.4.1 Sensitivity Analyses of the Horizontal Hydraulic Conductivity Field

Regarding the heterogeneity in horizontal hydraulic conductivity (K_{hf}), the aquifer surface was divided into 8 different K_{hf} zones (K_1, K_2, K_3, ...K_8) using a weighted nearest-neighbor interpolation (Fig. 8a). The distance of the well screen from the Salt Lake boundary and the well pumping rate are demonstrated with vertical and horizontal error bars in Fig. 8b, respectively. The transient movement of the saltwater toe (75% TDS isoline) is demonstrated for T=2462 day stress period with time step of 365 days, as shown in Fig. 8c. As shown, the maximum $\overline{SWI}$ value obtained by adjusting aquifer calibrated parameters corresponding to the current pumping strategy is approximately 3200 m.

Figure 9a shows the variation in iso-line TDS 75% between $T = 273$ days and $T = 2462$ days through the spatial variation of K_{hf}. The SEAWAT model was run to evaluate the effect of the variation in K_{hf} on $\overline{SWI}$ in the polluted area as shown in Fig. 9b. A linear sensitivity analysis of the $\overline{SWI}$ rate in response to variation in K_{hf} is applied and then compared to the case with a calibrated value of K_{hf}. Thus, 14 different combinations of K_{hf} in the 5 zones are examined to achieve the maximum variation in $\overline{SWI}$ length. Figure 9c shows the same behavior of a homogenous case where the increase in the spatial variation of calibrated K_{hf} (indicated by K_c) has less significant effects on the shape and movement of $\overline{SWI}$ length, Considering a non-uniform increase in K_c up to 2 times results in 700 (m) seaward advancement of the saltwater toe (see Fig. 9b). Moreover, in cases without changes in K_c in the lower part of aquifer (K_c 5, K_c 6, K_c 7) and maximum change in the upper part

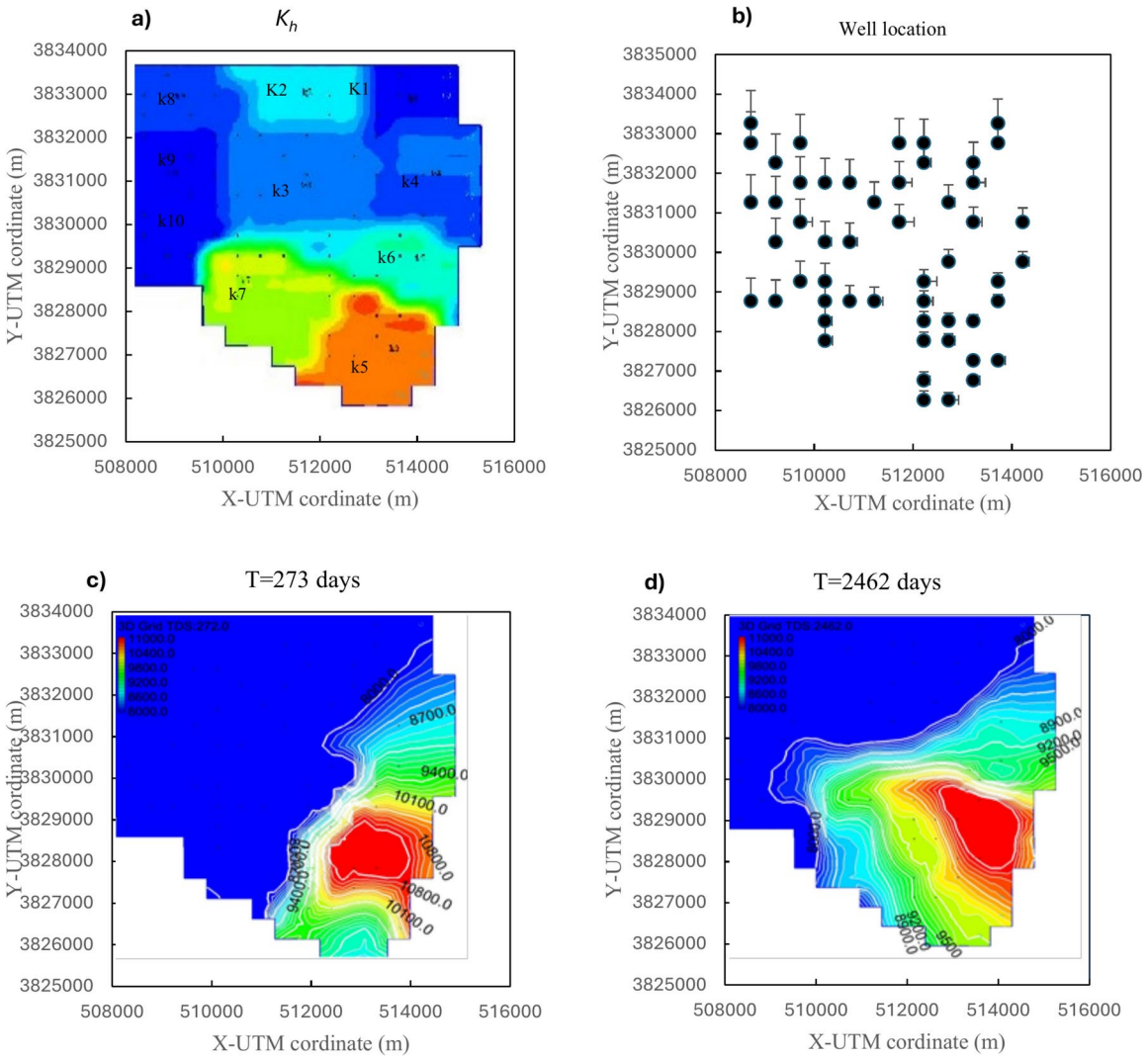

Fig. 8 a) Interpolated hydraulic conductivity based on observed data b) location and pumping rate (highlighted by error bar) of groundwater pumping well wells c, d) Transient variation of salinity wedge near the Salt Lake between T=273 days and T=2462 days

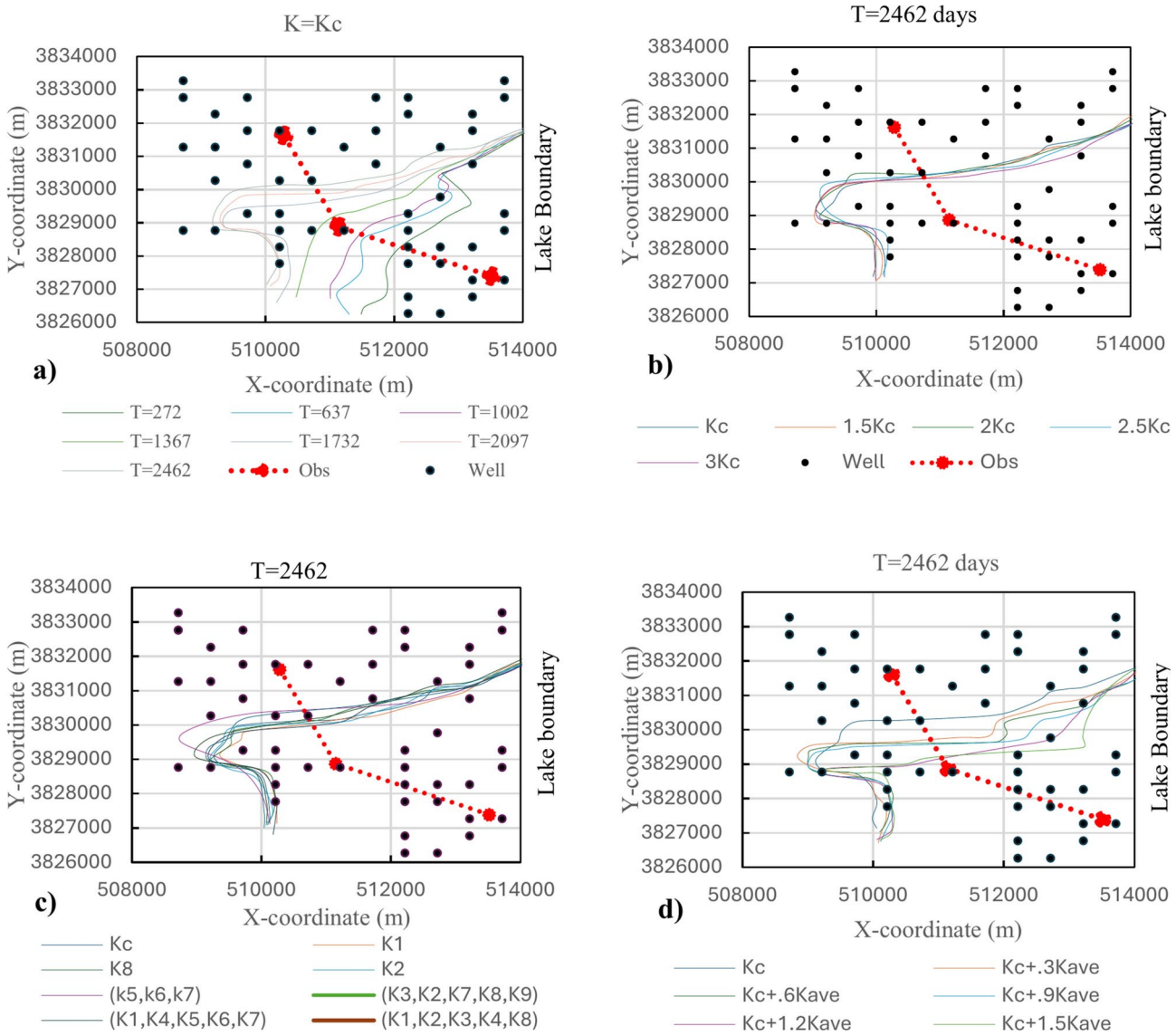

Fig. 9 Plot of the two-dimensional movement of the SWI wedge (isoline TDS 75%) for a stress period of 2462 days for different variations of calibrated K_c. The black points and red points are pumping wells and observation wells, respectively. The distance between the SWI wedge and observation points was demonstrated by red dashed line

(K_c 1, K_c 2, K_c 3, K_c 4), the maximum advancement of saltwater wedge in Y direction is observed. However, the total $\overline{SWI}$ length is smaller than that in the case with a constant increase in K_c as shown in Fig. 9c. In this case, a sensitivity analysis was applied by increasing K_c in different parts (K_1, $K_2 \ldots K_8$) up to 3 times of K_c (see Fig. 9d). The results indicate that the maximum horizontal and vertical movement of the saltwater toe is 600 m and 1100 m, respectively. Pumping from contaminated wells causes different $\overline{SWI}$ movement rates under different realizations of K_c, and thus results in uncertainty in management scenarios corresponding to the Pareto front.

The Pareto scenarios between $\overline{SWI}$ and the total pumping volume for a 6-year operation period are provided in Fig. 10. The robustness of these scenarios depends on the accuracy of the simulated TDS concentration which is a function of K_c. Therefore, the values of K_c in the upper part (K_{cu}) and lower part (K_{cl}) of the aquifer were increased up to 30% and then the Pareto curve was updated. K_{cu} and K_{cl} are the values of hydraulic conductivity in the upper and lower observation point, respectively. Figure 10 shows the Pareto curve related to 35 different realizations of hydraulic conductivity values (K_{cu} and K_{cl}).

As shown in Fig. 10, a 30% change in K_{cu} results in a 17% and 12% increase and decrease in $\overline{SWI}$, respectively. With increasing K_{cu}, the SWI advance to the upper part of the aquifer thus, the SWI area is reduced slightly in some Pareto scenarios. However, the total $\overline{SWI}$ length increases

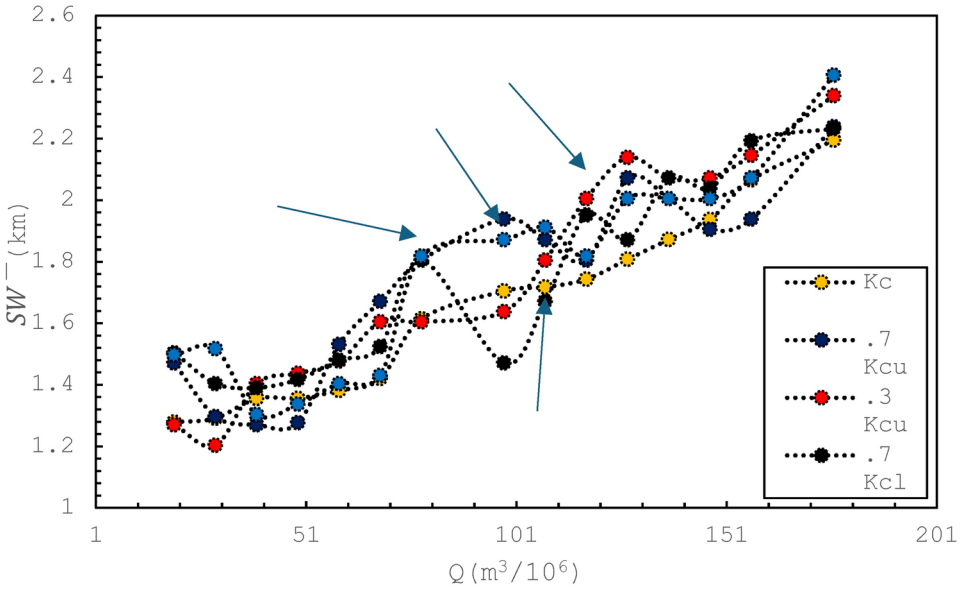

Fig. 10 The Pareto curve variation under different realization of K_c

with an increase in K_{cu} and K_{cl} for the majority of scenarios. Figure 10 indicates that K_c variation has a low impact on Pareto scenarios for the highest value of pumping rate (approximately more than 130 m^3/day) whereas, whereas the K_c impact on optimal scenarios near the current pumping rate (98 $m^3/10^6$) is significant. We selected some scenarios suggesting high pumping rates from the wells located around the observation points. For example, scenarios that extract water from Q_1 zone with a high pumping rate (approximately 3200 m^3/day) are extensively affected by the change in K_{cu} and hence these scenarios are not robust. However, the main source of uncertainty in the Pareto results corresponds to scenarios that are highly affected by K_c variations and hence these scenarios are selected for uncertainty analyses and to find robust scenarios using the IGDT theory.

4.4.2 Robustness Assessment of the Pareto Curve Based on Information Gap Decision Theory (IGDT)

To quantify the robustness of the optimal scenario based on the sensitivity analysis results obtained in the previous section, we used a non-dimensional form of parameters to describe the scenario. Therefore, the $\overline{SWI}$ length and the total extraction rate for each scenario were normalized by $2.45km$ and $188 \times 10^6 m^3$, being the maximum values of those parameters respectively. In the next step, the variation in $\overline{SWI}$ length due to the change in the realization of K_{hf} is quantified for each optimal scenario. Thus, the value of K_{hf} for 224 cells located between 3 observation points was determined by using linear interpolation and is presented in Table 6. To generate a new realization of K_{hf}, the cells value changed randomly for 11 parts of K_{hf} (see Table 6), and for each new realization, $\overline{SWI}$ length and Pareto curve are characterized using the MDT-NSGAII algorithm. In this study, the value of K_{hf} in the observation points has been varied between 0.3 and 0.7 of calibrated K_c with 0.01 interval. A total of 100 realizations were randomly generated and imported as the input to the SEAWAT model and then the Pareto curve was determined using the MDT-NSGAII algorithm. Based on trial and error, 15 non-dominated points were defined by assigning generations and population sizes of 290 and 210 to the NSGAII, respectively. To find the robustness threshold (r_c), the IGDT ranks the realizations in ascending order (from 1 to 100) with respect to their $\overline{SWI}$ length. Table 7 presents the robustness amount for $\overline{SWI}$ and extraction volume related to Pareto curve scenarios corresponding to different weights f= (5%, 10%…, 50%) and robustness threshold (r_c). Finally, the values of r_c are normalized by dividing them by the maximum objective values.

The value of obj_1 $(\overline{SWI})$ and $obj_2(Qtotal)$ considering 35% of f (based on stakeholder judgments) are considered 0.69 and 0.85, respectively.

To increase the speed of the IGDT model, the optimal scenarios of the Pareto solution are first selected for robustness assessment by IGDT. The main reason for this selection is that these points satisfy the utility functions of both the objectives. Figure 11 demonstrates the robustness values of the optimal scenario curve obtained by 70% of the scenarios and a f value of 35% (highlighted in Table 7).

4.4.3 Nash Bargaining Approach

To select the most preferred scenarios, the values of the non-dominated solutions are evaluated by the profit function of each farming area and the best scenarios are identified using a Nash conflict resolution model. Thus, the Nash values are

Table 6 The value of calibrated $K_{hf}(m/day)$ for each active cells of the SEAWAT grid using linear interpolation

6.5	6.5	6.5	11.6	11.6	11.6	11.6	11.6	4.7	4.7	4.7	4.7									
6.5	6.5	6.5	6.5	11.6	11.6	11.6	11.6	4.7	4.7	4.7	4.7									
6.5	6.5	6.5	6.5	11.6	11.6	11.6	11.6	4.7	4.7	4.7	4.7	7								
4.5	4.5	4.5	4.5	8.5	8.5	8.5	8.5	4.7	7	7	7	7	7							
4.5	4.5	4.5	4.5	8.5	8.5	8.5	8.5	7	7	7	7	7	7	7						
4.5	4.5	4.5	4.5	8.5	8.5	8.5	8.5	7	7	7	7	7	7	7	7					
4.5	4.5	4.5	4.5	8.5	8.5	8.5	8.5	7	7	7	7	7	7	7	7	7				
2	4.5	4.5	4.5	8.5	8.5	8.5	8.5	7	7	7	14.6	14.6	7	7	7	7	7			
2	2	2	2	12	12	12	12	12	14.6	14.6	14.6	14.6	14.6	14.6	14.6	14.6	14.6	14.6		
2	2	2	26.7	26.7	26.7	12	12	14.6	14.6	14.6	14.6	14.6	14.6	14.6	14.6	14.6	14.6	14.6	14.6	
2	2	2	26.7	26.7	26.7	26.7	26.7	26.7	14.6	14.6	14.6	14.6	14.6	14.6	14.6	14.6	14.6	14.6	14.6	14.6
			26.7	26.7	26.7	26.7	26.7	26.7	34	34	34	34	34	34	34	34	34	34	34	34
			26.7	26.7	26.7	26.7	26.7	26.7	34	34	34	34	34	34	34	34	34	34	34	34
				26.7	26.7	26.7	26.7	34	34	34	34	34	34	34	34	34	34	34	34	34
							26.7	34	34	34	34	34	34	34	34	34	34	34	34	34

Table 7 The lower and upper limit for Pareto curve components in IGDT

Objective	$obj_1(m^3/10^6)$	$obj_2\ (\bar{SWI}\ (km))$
obj_{max}	176.46	2.27
obj_{min}	19.60	1.32
$f(\%)$	r_c	r_c
0.05	0.95	0.97
0.10	0.91	0.95
0.15	0.86	0.93
0.20	0.82	0.91
0.25	0.77	0.89
0.30	0.73	0.87
0.35	0.69	0.85
0.40	0.64	0.83
0.45	0.60	0.81
0.50	0.55	0.79

calculated for all robust Pareto scenarios obtained from the IGDT approach. There are 5 stakeholders near the Salt Lake including the agricultural zones of Malekan, Dolatabad, Noran, Momenabad and Serajeh with different land use and pumping rates.

$Q_{Pareto} = (Q_1, Q_2, Q_3, Q_4, Q_5)$ is the vector of scenarios in the Pareto front while $Q_{stakeholder} = (Q_{ma}, Q_d, Q_n, Q_m, Q_s)$ is the vector of the total water demand corresponding to the 5 stakeholders. Although, both Q_{Pareto} and $Q_{stakeholder}$ are the optimal scenarios and their uncertainty is assessed by IGDT for robustness purposes in the last section, the priority of $Q_{stakeholder}$ for stakeholders of 5 agricultural zones is evaluated in terms of NASH index. The minimum pumping rate to satisfy 50% of the current profit of 5 zone is $Q_{stakeholder(50\%)}$ = (3400 m^3/day, 11,400 m^3/day, 8100 m^3/day, 16,300 m^3/day, 34,450 m^3/day). Moreover, the maximum allowed TDS concentration for each zone related to land use is allowed between 7100 and 7500 mg/lit to provide a minimum groundwater demand of 50%. The values of the Nash products for the Pareto scenario (Q_{Pareto}) are shown in Fig. 12a.

Based on Nash product values, scenarios 10 and 12 are the best scenarios whereas scenarios 8 and 10 are the most robust scenarios through the Pareto front that satisfy only 35% of the mean Nash index (1.45). Scenario 10 allocates groundwater fairly based on the maximum discharge of the 5 agricultural regions.

It can be understood that Nash products tend to select scenarios that cause a relatively uniform SWI zone (SWI zone illustrated in Fig. 10d), similar to the current SWI wedge. The reason for this complexity is that, in this case, the TDS limit is satisfied for all 5 agricultural zones. In robust scenarios, the priority of a high extraction rate is pumping from wells adjacent to the observation point (Serajeh area). For the agricultural zone of Momenabad, all scenarios 1–15 are

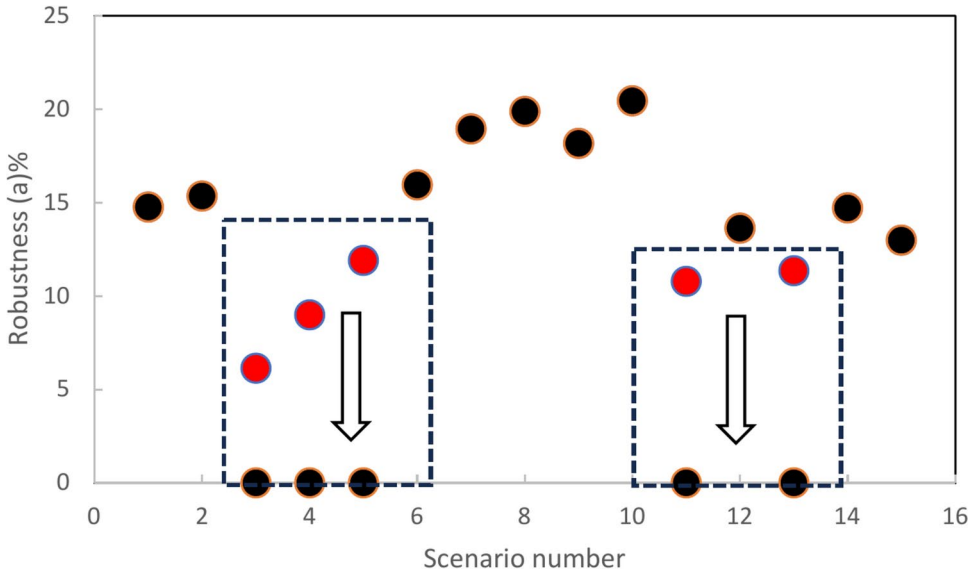

Fig. 11 Robustness of the optimal scenarios for objective $\overline{SWI}$ (all points are corresponding $f = 35\%$) the whole red points have a robustness value less than threshold and hence, their robustness considered zero)

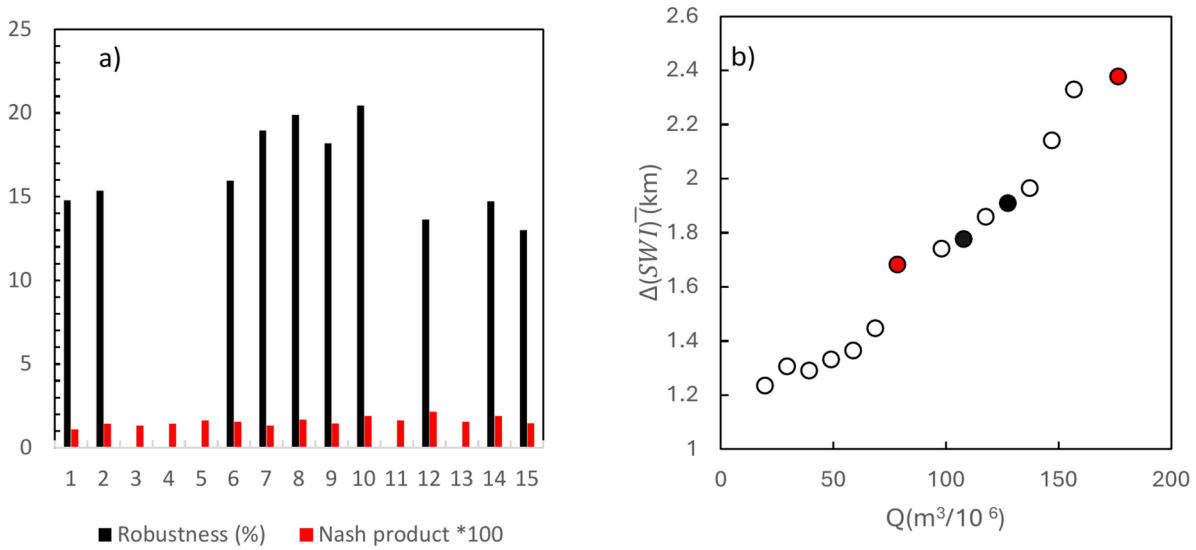

Fig. 12 The value of robustness versus Nash values for optimal Pareto scenarios, a) Robustness and Nash values d) Pareto curve for the calibrated value of K_{cf}

acceptable because this area is located far from the Lake boundary; hence the TDS concentration is less than 7500 mg/l. On the other hand, the robustness of the scenario with high values of extraction rate (more than $130 \times 10^6 m^3$) is less than the threshold (the total pumping volume proposed by scenario 12 is approximately 11.5% less than that of scenario 10). In total scenario 12 reached 75% of the highest Nash product while ensuring the robustness threshold; hence this scenario is more desirable from the stakeholders' perspective. The main objective of this study is to select the most preferable scenarios by stakeholders rather than the most robust scenario (only the robustness threshold is satisfied) thus, maximizing the robustness value is the second important objective.

5 Conclusions

This study constructs a framework to examine the impact of uncertainty in calibrated horizontal hydraulic conductivity on Pareto optimal scenarios in a coastal aquifer. The most robust and preferable scenarios are determined by applying uncertainty analyses and bargaining approach to the Pareto solution, respectively. In this regard the SEAWAT model is used to simulate the time-variant saltwater intrusion (SWI) wedge under different realizations of the horizontal hydraulic conductivity field (K_{hf}). An efficient surrogate model of the M5 decision tree (MDT) is trained with different pumping rates patterns in 55 production wells and SWI length. The Pareto optimal scenarios of the total pumping volume

and SWI length are calculated by coupling the NSGAII to the MDT algorithm. After verifying the Pareto solution, the uncertainty of scenarios associated with K_{hf} is assessed using information-gap decision theory (IGDT). Finally, the conflict resolution between the stakeholders of the aquifer is solved by calculating the Nash index of the robust optimal scenarios. The results show that the linear regression relations generated by MDT can predict a SWI length that is 97% correlated with those simulated by SEAWAT, whereas the coupled MDT-NSGAII algorithm requires only 4% of the processing time compared with SEAWAT-NSGAII. After applying the robustness criteria of the IGDT theory to the Pareto front, the mean total extraction rate is approximately 11.5% less than certain Pareto scenarios obtained by the simulation optimization model, which highlights the significant impact of considering uncertainty on optimal scenarios. Moreover, the most robust scenarios suggest increasing the extraction rate from the pumping wells located near the observation points and far from the Salt Lake boundary. The result of the Nash bargaining approach suggests selecting the optimal scenarios that lead to a uniform SWI wedge parallel to the Salt Lake boundary, whereas the simulated SWI wedge for optimal scenarios based on the Pareto solution is somewhat sharp. Thus, the most preferable scenario for the Pareto solution is the most robust scenario that satisfies 50% of the Nash product for all stakeholders in the aquifer. The findings of this research are valid for a real case study of the Qom-Kahak aquifer where over-extraction from 55 pumping wells causes SWI in the agricultural zone. However, the proposed methodology could be applied to the management of other real case studies and for different boundary conditions where calibrated parameters are uncertain.

Supplementary Information The online version contains supplementary material available at https://doi.org/10.1007/s41748-025-00585-3.

Funding Open access funding provided by Università degli Studi di Trieste within the CRUI-CARE Agreement.

Data availability The author confirms that the data supporting the finding of the study are available within the article and its supplementary material. Raw data that supports the findings of this study are available from the corresponding author, upon reasonable request. This article contains the following extended raw data: Aquifer geology and bed rock topography information.xlsx. Groundwater heads in observation points.xlsx. Groundwater chlorine and TDS concentration in observation points.xlsx. Remote sensing images of the study area. Consultant_report_2016.docx (initial consultancy report). Reference_list.docx (reference list for observation point).

Open Access This article is licensed under a Creative Commons Attribution 4.0 International License, which permits use, sharing, adaptation, distribution and reproduction in any medium or format, as long as you give appropriate credit to the original author(s) and the source, provide a link to the Creative Commons licence, and indicate if changes were made. The images or other third party material in this article are included in the article's Creative Commons licence, unless indicated otherwise in a credit line to the material. If material is not included in the article's Creative Commons licence and your intended use is not permitted by statutory regulation or exceeds the permitted use, you will need to obtain permission directly from the copyright holder. To view a copy of this licence, visit http://creativecommons.org/licenses/by/4.0/.

References

Abd-Elaty I, Kushwaha NL, Grismer ME, Elbeltagi A, Kuriqi A (2022) Cost-effective management measures for coastal aquifers affected by saltwater intrusion and climate change. Sci Total Environ 836:155656. https://doi.org/10.1016/j.scitotenv.2022.155656. (**Elsevier BV**)

Akter T, Hoque MA-A, Mukul SA, Pradhan B (2024) coastal flood induced salinity intrusion risk assessment using a spatial multi-criteria approach in the South-Western Bangladesh. In Earth Syst Environ. https://doi.org/10.1007/s41748-024-00399-9. (**Springer Science and Business Media LLC**)

Alnahit AO, Mishra AK, Khan AA (2022) Stream water quality prediction using boosted regression tree and random forest models. Stochastic Environ Res Risk Assess 36(9):2661–2680. https://doi.org/10.1007/s00477-021-02152-4. (**Springer Science and Business Media LLC**)

Christelis V, Kopsiaftis G, Regis RG, Mantoglou A (2023) An adaptive multi-fidelity optimization framework based on co-Kriging surrogate models and stochastic sampling with application to coastal aquifer management. Adv Water Resour 180:104537. https://doi.org/10.1016/j.advwatres.2023.104537. (**Elsevier BV**)

Deb K (2002) A fast and elitist multi-objective genetic algorithm: NSGA-II. IEEE Trans Evol Comput 6(2):182–197

Durantin C, Rouxel J, Désidéri J-A, Glière A (2017) Multifidelity surrogate modeling based on radial basis functions. Struct Multidisciplin Optimiz 56(5):1061–1075. https://doi.org/10.1007/s00158-017-1703-7. (**Springer Science and Business Media LLC**)

Fan Y, Xin J, Yang L, Zhou J, Luo C, Zhou Y, Zhang H (2024) Optimization method for the length of the outsourcing concrete working plane on the main arch rib of a rigid-frame arch bridge based on the NSGA-II algorithm. Structures 59:105767. https://doi.org/10.1016/j.istruc.2023.105767. (**Elsevier BV**)

Feist SE, Hoque MA, Ahmed KM (2022) Coastal salinity and water management practices in the Bengal delta: a critical analysis to inform Salinisation risk management strategies in Asian deltas. Earth Syst Environ 7(1):171–187. https://doi.org/10.1007/s41748-022-00335-9. (**Springer Science and Business Media LLC**)

Forrester DI, Dumbrell IC, Elms SR, Paul KI, Pinkard EA, Roxburgh SH, Baker TG (2020) Can crown variables increase the generality of individual tree biomass equations? Trees 35(1):15–26. https://doi.org/10.1007/s00468-020-02006-6. (**Springer Science and Business Media LLC**)

Frank E, Wang Y, Inglis S, Holmes G, Witten IH (1998) Mach Learn 32(1):63–76. https://doi.org/10.1023/a:1007421302149. (**Springer Science and Business Media LLC**)

Ghodsi SH, Kerachian R, Estalaki SM, Nikoo MR, Zahmatkesh Z (2016) Developing a stochastic conflict resolution model for urban runoff quality management: application of info-gap and bargaining theories. In J Hydrol 533:200–212. https://doi.org/10.1016/j.jhydrol.2015.11.045. (**Elsevier BV**)

Guo W & Langevin CD (2002) User's guide to SEAWAT; a computer program for simulation of three-dimensional variable-density ground-water flow. In Open-File Report. US Geological Survey. https://doi.org/10.3133/ofr01434

Harbaugh AW, Banta ER, Hill MC & McDonald MG (2000) MODFLOW-2000, The U.S. Geological Survey modular ground-water model: User guide to modularization concepts and the ground-water flow process. In Open-File Report. US Geological Survey. https://doi.org/10.3133/ofr200092

Houben GJ, Stoeckl L, Mariner KE, Choudhury AS (2018) The influence of heterogeneity on coastal groundwater flow - physical and numerical modeling of fringing reefs, dykes and structured conductivity fields. Adv Water Resour 113:155–166. https://doi.org/10.1016/j.advwatres.2017.11.024. (**Elsevier BV**)

Hussain MS, Abd-Elhamid HF, Javadi AA, Sherif MM (2019) Management of seawater intrusion in coastal aquifers: a review. Water 11(12):2467. https://doi.org/10.3390/w11122467. (**MDPI AG**)

Imaz-Lamadrid MA, Wurl J, Ramos-Velázquez E, Guadalupe Gutiérrez-González MV (2023) SWIVI: A climate change-oriented multi-parametric framework to enhance saltwater intrusion vulnerability assessment. Groundwater Sustain Dev 23:101027. https://doi.org/10.1016/j.gsd.2023.101027. (**Elsevier BV**)

Jiang X, Ma R, Wang Y, Gu W, Lu W, Na J (2021) Two-stage surrogate model-assisted Bayesian framework for groundwater contaminant source identification. J Hydrol 594:125955. https://doi.org/10.1016/j.jhydrol.2021.125955. (**Elsevier BV**)

Ketabchi H, Jahangir MS (2021) Influence of aquifer heterogeneity on sea level rise-induced seawater intrusion: a probabilistic approach. J Contaminant Hydrol 236:103753. https://doi.org/10.1016/j.jconhyd.2020.103753. (**Elsevier BV**)

Kourakos G, Mantoglou A (2009) Pumping optimization of coastal aquifers based on evolutionary algorithms and surrogate modular neural network models. Adv Water Resour 32(4):507–521

Langevin CD, Guo W (2005) MODFLOW/MT3DMS–based simulation of variable-density ground water flow and transport. Groundwater 44(3):339–351. https://doi.org/10.1111/j.1745-6584.2005.00156.x. (**Wiley**)

Li L, Qiao J, Yu G, Wang L, Li H-Y, Liao C, Zhu Z (2022) Interpretable tree-based ensemble model for predicting beach water quality. Water Res 211:118078. https://doi.org/10.1016/j.watres.2022.118078. (**Elsevier BV**)

Luo J, Ma X, Ji Y, Li X, Song Z, Lu W (2023) Review of machine learning-based surrogate models of groundwater contaminant modeling. Environ Res 238:117268. https://doi.org/10.1016/j.envres.2023.117268. (**Elsevier BV**)

Mahboobi H, Shakiba A, Mirbagheri B (2023) Improving groundwater nitrate concentration prediction using local ensemble of machine learning models. J Environ Manag 345:118782. https://doi.org/10.1016/j.jenvman.2023.118782. (**Elsevier BV**)

McDonald MG (1988) A modular three-dimensional finite-difference ground-water flow model. Techniques of Water-Resources Investigations of the United States Geological Survey

Nash JF, join (1950) The bargaining problem. Econometrica 18(2):155. https://doi.org/10.2307/1907266. (**JSTOR**)

Pisinaras V, Paraskevas C, Panagopoulos A (2021) Investigating the effects of agricultural water management in a mediterranean coastal aquifer under current and projected climate conditions. Water 13(1):108. https://doi.org/10.3390/w13010108. (**MDPI AG**)

Pool M, Post VEA, Simmons CT (2015) Effects of tidal fluctuations and spatial heterogeneity on mixing and spreading in spatially heterogeneous coastal aquifers. Water Resour Res 51(3):1570–1585. https://doi.org/10.1002/2014wr016068. (**American Geophysical Union (AGU)**)

Qiang J, Zhang S, Liu H, Zhu X, Zhou J (2024) A construction strategy of Kriging surrogate model based on Rosenblatt transformation of associated random variables and its application in groundwater remediation. J Environ Manag 349:119555. https://doi.org/10.1016/j.jenvman.2023.119555. (**Elsevier BV**)

Ranjbar A, Mahjouri N (2019) Multi-objective freshwater management in coastal aquifers under uncertainty in hydraulic parameters. Nat Resour Res 29(4):2347–2368. https://doi.org/10.1007/s11053-019-09585-3. (**Springer Science and Business Media LLC**)

Ranjbar A, Mahjouri N, Cherubini C (2020) Development of an efficient conjunctive meta-model-based decision-making framework for saltwater intrusion management in coastal aquifers. J Hydro-Environ. https://doi.org/10.1016/j.jher.2019.11.005

Riva M, Guadagnini A, Dell'Oca A (2015) Probabilistic assessment of seawater intrusion under multiple sources of uncertainty. Adv Water Resour 75:93–104. https://doi.org/10.1016/j.advwatres.2014.11.002. (**Elsevier BV**)

Roy DK, Datta B (2018) A review of surrogate models and their ensembles to develop saltwater intrusion management strategies in coastal aquifers. Earth Syst Environ 2(2):193–211. https://doi.org/10.1007/s41748-018-0069-3. (**Springer Science and Business Media LLC**)

Roy DK, Leslie DL, Reba ML, Hashem AA, Bellis E, Nowlin J (2024) Optimizing the quantity of recharge water into a sedimentary aquifer through infiltration galleries using a surrogate assisted coupled simulation–optimization approach. J Hydrol 635:131183. https://doi.org/10.1016/j.jhydrol.2024.131183. (**Elsevier BV**)

Saad S, Javadi AA, Farmani R, Sherif M (2023) Efficient uncertainty quantification for seawater intrusion prediction using Optimized sampling and Null Space Monte Carlo method. J Hydrol 620:129496. https://doi.org/10.1016/j.jhydrol.2023.129496. (**Elsevier BV**)

Secci D, Godoy VA, Gómez-Hernández JJ (2024) Physics-Informed Neural Networks for solving transient unconfined groundwater flow. Comput Geosci 182:105494. https://doi.org/10.1016/j.cageo.2023.105494. (**Elsevier BV**)

Shahabi A, Tahvildari N (2024) A deep-learning model for rapid spatiotemporal prediction of coastal water levels. Coastal Eng 190:104504. https://doi.org/10.1016/j.coastaleng.2024.104504. (**Elsevier BV**)

Shehab SA, Darwish A, Hassanien AE (2023) Water quality classification model with small features and class imbalance based on fuzzy rough sets. Environ Dev Sustain. https://doi.org/10.1007/s10668-023-03916-4. (**Springer Science and Business Media LLC**)

Song J, Yang Y, Wu J, Wu J, Sun X, Lin J (2018) Adaptive surrogate model based multiobjective optimization for coastal aquifer management. J Hydrol 561:98–111. https://doi.org/10.1016/j.jhydrol.2018.03.063. (**Elsevier BV**)

Tyan M, Nguyen NV, Lee J-W (2014) Improving variable-fidelity modelling by exploring global design space and radial basis function networks for aerofoil design. Eng Optimiz 47(7):885–908. https://doi.org/10.1080/0305215x.2014.941290. (**Informa UK Limited**)

Uddin MG, Nash S, Rahman A, Olbert AI (2023) Assessing optimization techniques for improving water quality model. J Clean Prod 385:135671

Uddin MG, Imran MH, Sajib AM, Hasan MA, Diganta MTM, Dabrowski T, Olbert AI, Moniruzzaman M (2024) Assessment of human health risk from potentially toxic elements and predicting groundwater contamination using machine learning approaches. J Contaminant Hydrol 261:104307. https://doi.org/10.1016/j.jconhyd.2024.104307. (**Elsevier BV**)

Wang Z, Lu W, Chang Z, Luo J (2023) A combined search method based on a deep learning combined surrogate model for groundwater DNAPL contamination source identification. J Hydrol 616:128854. https://doi.org/10.1016/j.jhydrol.2022.128854. (**Elsevier BV**)

Werner AD (2017) Correction factor to account for dispersion in sharp-interface models of terrestrial freshwater lenses and active

seawater intrusion. Adv Water Resourc 102:45–52. https://doi.org/10.1016/j.advwatres.2017.02.001. (**Elsevier BV**)

Yin J, Tsai FT-C (2018) Saltwater scavenging optimization under surrogate uncertainty for a multi-aquifer system. J Hydrol 565:698–710. https://doi.org/10.1016/j.jhydrol.2018.08.021. (**Elsevier BV**)

Yin J, Huang Y, Lu C, Liu Z (2024) Uncertainty-based saltwater intrusion prediction using integrated Bayesian machine learning modeling (IBMLM) in a deep aquifer. J Environ Manage 354:120252. https://doi.org/10.1016/j.jenvman.2024.120252. (**Elsevier BV**)

Younes A, Fahs M, Ataie-Ashtiani B, Simmons CT (2020) Effect of distance-dependent dispersivity on density-driven flow in porous media. J Hydrol 589:125204. https://doi.org/10.1016/j.jhydrol.2020.125204. (**Elsevier BV**)

Zhou Q, Wu Y, Guo Z, Hu J, Jin P (2020) A generalized hierarchical co-Kriging model for multi-fidelity data fusion. Struct Multidisciplin Optimiz 62(4):1885–1904. https://doi.org/10.1007/s00158-020-02583-7. (**Springer Science and Business Media LLC**)